

# Effect of matrix cracks and delamination on extension-twist coupling of thin pretwisted composite strips



Santosh B. Salunkhe<sup>a</sup>, C.V. Singh<sup>b</sup>, P.J. Guruprasad<sup>a,\*</sup>

<sup>a</sup> Department of Aerospace Engineering, Indian Institute of Technology Bombay, Mumbai 400076, India

<sup>b</sup> Materials Science and Engineering, University of Toronto, 184 College St., Suite 140, Toronto, Canada

## ARTICLE INFO

### Article history:

Received 21 February 2017

Revised 12 June 2017

Accepted 19 July 2017

Available online 21 July 2017

### Keywords:

Composite structure

Pretwist

Trapeze effect

Matrix cracks

Delamination

## ABSTRACT

An asymptotically exact cross-sectional model coupled with geometrically nonlinear one-dimensional (1D) theory is developed for a thin composite strip in the presence of defects. Two types of defects are considered: intralaminar cracks and interlaminar cracks. Model development is based on the dimensional reduction of laminated shell theory to nonlinear 1D theory using the variational asymptotic method. The cross-sectional nonlinearity accounts for matrix cracks, quantified in terms of crack density and delamination, quantified in terms of the delamination width. For modeling intralaminar cracks continuum damage mechanics based framework is used along with computational micromechanics to account for intralaminar cracks in laminate plies in different orientations. Delamination modeling follows a methodology adapted from the sublaminar approach. The model developed is used to investigate the effect of defects on the trapeze effect – nonlinear axial-twist coupling in strip with Winckler kind of layup. It was found that cracks in transverse plies enhance the trapeze effect; on the contrary, symmetric edge mid-surface delamination leads to decrease in the coupling effect. This contrarian behavior of the two types of defects on the trapeze effect is explained on the effect these defects have on the various cross-sectional coupling stiffness terms influencing the coupling behavior. Model predictions are presented for strip stiffness degradation due to matrix cracks and delamination.

© 2017 Elsevier Ltd. All rights reserved.

## 1. Introduction

Helicopter rotor blade degrees of freedom involves pitching, flapping and lead-lag motion. Traditionally, these motions have been accommodated by fully articulated bearing and hinge based tail-rotor hub design [1]. Bearing and hinge based rotor design is, however, mechanically complex and unnecessarily transfers the centrifugal loads to the hinges and the rotor hub. More recently, this traditional form of design has been replaced by bearingless and hingless flexbeam based rotor design [2]. In bearingless and hingless design, flexbeams, made of fiber reinforced composite materials, are typically used to connect diametrically opposite rotor blades through the hub to take on the centrifugal force. The flexbeams are typically strip like structures and provide the necessary elastic coupling to accommodate the various motions of the rotor blade. These structures are consistently subjected to high magnitudes of centrifugal and bending loads and hence they are designed such that their thickness decreases away from the rotor

hub. This is achieved during the manufacturing by ply-dropping technique. High centrifugal and bending load and discontinuities at internal ply-drop locations lead to intra- and inter-laminar cracks in these structures. The focus in this work is to model intra- and inter-laminar crack(s) in anisotropic pretwisted strip like configuration typically used as flexbeam structures. The aim is not to model an exact flexbeam structure but to develop a general methodology by considering an anisotropic pretwisted strip, which can be eventually used to model a flexbeam with ply-drops. It is envisaged that the proposed model provides a unified approach to account for damage within the Variational Asymptotic Method (VAM) based strip analysis to capture the overall stiffness degradation – at lamina and strip level and deformation.

Multiple matrix cracking, also known as “intralaminar cracking”, is usually the first form of damage observed during experiments on composite laminates subjected to uniaxial loading [3]. Although it does not cause laminate failure instantly, it causes degradation in the stiffness properties of a structure and provides pathways for other forms of damage, such as delamination. The subject of intralaminar cracking has been quite extensively studied in the past few decades [4–10]. For cross-ply laminates, in particular, the analysis approaches have become quite mature. In

\* Corresponding author.

E-mail address: [pjguru@aero.iitb.ac.in](mailto:pjguru@aero.iitb.ac.in) (P.J. Guruprasad).

general, matrix crack modeling strategies can be divided into the following: (i) shear lag based approaches [11]; (ii) variational methods [5,12,13]; (iii) crack opening displacement (COD) and crack face sliding displacement (CSD) models [14–17]; and (iv) continuum damage mechanics [18–21]. Initially, most of the work was limited to cross-ply laminates. This focus on cross-ply laminates led to the development of 1D shear-lag approach. Subsequently, there have been number of improvement and refinements to the 1D shear-lag approach [22,23]. Variational approach based methods typically considered 2D boundary value problem to determine the statically admissible stress fields and their perturbation within the lamina in the undamaged and cracked state [24], respectively. COD and CSD based approaches can be accommodated within the laminate theory to determine the laminate stiffness and compliance matrix along with the hygrothermal coefficients. Challenge, however, is in using the above approaches in a structural analysis involving matrix crack progression with deformation since they involve explicit representation of the underlying laminate microscale description. An extensive review highlighting the development of various models and their relative merits and demerits is presented in [25].

Continuum damage mechanics (CDM) approach offers an alternative compared to the other methods discussed above. Models based on CDM approximate an underlying cracked laminate with an equivalent homogenized continuum. Talreja [4] was among the first to propose a CDM approach to model damage in fiber reinforced composites. The model proposed additive decomposition of the constitutive matrix of laminate containing matrix cracks into constitutive matrix of undamaged laminate and a matrix accounting for damage leading to the overall reduction in the stiffness of the laminate. Subsequent models, for example [26–29], focused on including the effect of ply level matrix crack development and evolution, constraint effect and nonlinear behavior between damage parameter and crack density. For general laminates, only a few models, such as [26] can yield satisfactory predictions for stiffness changes due to transverse cracking. The model by Li et al. [26] is a modification of Talreja's continuum damage model [18] and it carries the necessary physical basis and predictive capability, in addition to the simplicity necessary for numerical implementation. In the present work, we shall use CDM approach for calculating stiffness changes in lamina due to multiple matrix cracking. The damage variables and constants appearing in the CDM model will be determined from computational micromechanics using finite element method (FEM) as proposed by Singh and Talreja [30]. The homogenized material properties of the laminate will then be used in the strip analysis.

Interlaminar cracking or delamination between two layers of the laminate is quite detrimental and may directly cause component failure. It is thus very important to develop analysis procedures to account for this damage mode. It should be noted that matrix cracks happen at the material level while delamination is a structural level failure. Hence it is only appropriate that delamination effects are captured during structural modeling of the strip. Many analytical and numerical models are available in the literature for composite laminates with delaminations. A detailed review about delamination modeling in beams and their effects on the structural dynamics are provided by Della et al. [31]. It is observed that the majority of the available methods/techniques can be categorized into two classes: (a) region approach; (b) layer-wise approach. Further, the region approach model can be divided into free and constrained mode models. Mujumdar et al. [32] made the comparison between these modes with experimental data and brought out the salient features between these two approaches. For complete perspective on delamination model, the reader is referred to Kim et al. [33] for quasi 3D finite element method of delamination modeling, Wang [34] for free mode with classical

beam theory, Barbero et al. [35] and Saravanas et al. [36] for layer-wise approach, Shen et al. [37] for detailed experimental results, Armanios et al. [38] for sublaminar approach, Li et al. [39] for analytical model to understand the extension twist coupling, Chakraborty et al. [40] for 3 noded finite element model, Averill [41] and Kim et al. [42] for zig-zag theory and Cho et al. [43] for higher order zig-zag theory. More recently, Carrera unified formulation [44,45] was used to investigate the dynamic behavior of laminated composites with partial delaminations [46].

Over the last decade variational asymptotic method has emerged as a very effective and efficient mathematical framework to model dimensionally reducible composite structures like beams, strips, plates and shells [47–49]. The mathematical framework was originally proposed by Berdichevsky [50] and later adapted to structural engineering problems by Hodges [51,52]. A primary advantage of the framework is that it is free from *ad hoc* assumptions prevalent in other dimensionally reducible structure models. Due to the inherent variational form of the problem formulation it is easy to implement the framework in FEM. Analytical modeling can be easily developed for structures with simple geometries. The mathematical framework has demonstrated the capability to capture nonlinear phenomenon like trapeze effect [53] in strips and Brazier effect [54] in thin walled hollow tubes; additionally, beams having material and geometrical nonlinearity have been successfully modeled [55,56]. Recently, VAM based models have also been used to study the effect of damage in strips [57] and rotor blades [58].

The primary focus in this work is on the development of a modeling strategy to include the effects of both matrix cracks and delamination in pretwisted anisotropic strips. The aim is to investigate the trapeze effect in the presence of these defects. Trapeze effect in damaged strip has not been discussed much except in a few studies, e.g. [59,60,57]. Even in these studies it is limited to investigating the effect of only delamination on the trapeze effect in pretwisted strips.

In the present work, the structural model is based on the variational asymptotic method. Matrix cracks and delamination are introduced into the model through ply stiffness degradation and sub-laminar approach, respectively. Continuum damage mechanics coupled with computational micromechanics is adopted to capture ply stiffness degradation. The degraded stiffness terms are then carried forward in the strip modeling. Delamination is naturally captured by the sublaminar approach within the VAM framework. Nonlinear cross-sectional analysis is limited to the case of anti-symmetric Winckler layup strips in this work. This is not a limitation of the model or the mathematical framework. The layup restriction is primarily to reduce the mathematical complexity and demonstrate through analytical solutions the capability of the model to capture the damage effects on the trapeze behavior. The final result obtained from this formulation contains both linear as well as nonlinear stiffness terms that account for both intralaminar and interlaminar cracks.

## 2. Stiffness degradation model for matrix cracking in a general laminate

A lamina has low stiffness properties transverse to the fiber direction. Therefore, when a composite laminate made from a mix of on-axis and off-axis plies is loaded in tension, the plies transverse to the loading axis begin developing intralaminar cracks. These ply cracks usually grow unstably through the ply thickness and are stopped at the interface between plies of different orientations. A typical crack, once fully developed through the ply thickness, starts developing along the fiber directions traversing the entire lamina width. After the initiation of first ply crack,

more and more cracks start forming in-between existing cracks, and quickly form a somewhat periodic array of fully developed cracked surfaces parallel to the fiber direction in a given lamina. A representative schematic of this phenomenon is shown in Fig. 1 illustrating the ply cracking in a  $[0/90/-\theta/+\theta]_s$  laminate under tensile loading along  $x_1$  direction.

The immediate effect of ply cracks is to cause reduction in the thermoelastic properties of the laminate. Many analytical models have been developed to describe the thermoelastic constants of the damaged laminate as a function of crack density. The continuum damage mechanics (CDM) model proposed by Li et al. [26], which is applicable for laminates with an arbitrary layup, is used in the present work. There are also three major differences between this approach and the CDM based method proposed by Talreja [4] that makes it amenable for the problem considered in this work. In this approach it is not necessary to define a tensor-valued damage as an internal variable in a continuum mechanics formulation considering the whole laminate as a representative volume element. Such a representation involves tedious determination of damage-related material constants for every laminate under consideration either through experiments or computational micromechanics. The model proposed by Li et al. [26] overcomes this difficulty by an approach that defines a scalar damage parameter at the lamina level capable of accounting the influence of adjacent laminae of different fiber directions. Further, it obviates the necessity to consider empirical factor necessary to take into account the constraints on the cracked surface displacements depending on the lamina position in a laminate. The model proposed by Li et al. [26] also does not lead to all the effective material properties being proportional to crack density and thus applicable to a wider range of crack density. Following the ideas proposed in [26], the cracks are considered to be periodic and fully developed through the lamina thickness and width. In such a lamina, the stiffness properties of the cracked laminate is determined to be

$$\begin{bmatrix} A & B \\ B & D \end{bmatrix} = \sum_{k=1}^N \bar{Q}_k \begin{bmatrix} z_k - z_{k-1} & \frac{1}{2}(z_k^2 - z_{k-1}^2) \\ \frac{1}{2}(z_k^2 - z_{k-1}^2) & \frac{1}{3}(z_k^3 - z_{k-1}^3) \end{bmatrix} \quad (1)$$

In Eq. (1),  $N$  is the total number of laminae in the layup and  $\bar{Q}_k$  the stiffness matrix of the  $k$ th layer lamina transformed in the laminate (global) coordinate system. Lamina stiffness transformation is given by

$$\bar{Q}_k = T^{-1} Q_k R T R^{-1} \quad (2)$$

where,

$$Q_k = Q_k^0 + Q_k^D w_k \quad (3)$$

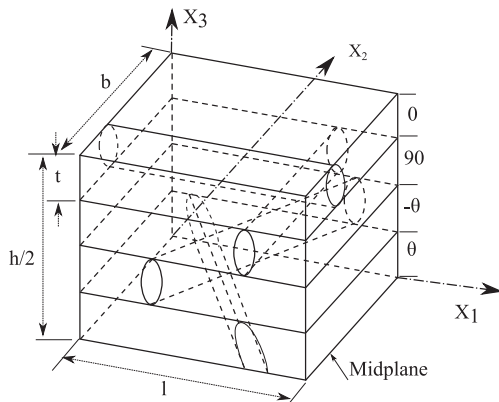


Fig. 1. The 3D geometry of repeating volume element of multi-directional laminate containing ply cracks in multiple direction.

Here,  $T$  is the coordinate transformation matrix for a lamina with orientation  $\theta$  with respect to the loading direction and is given by

$$T = \begin{bmatrix} \cos^2(\theta) & \sin^2(\theta) & 2 \cos(\theta) \sin(\theta) \\ \sin^2(\theta) & \cos^2(\theta) & -2 \cos(\theta) \sin(\theta) \\ -\cos(\theta) \sin(\theta) & \cos(\theta) \sin(\theta) & \cos^2(\theta) - \sin^2(\theta) \end{bmatrix} \quad (4)$$

and

$$Q_k^0 = \begin{bmatrix} \frac{E_1^0}{1-\nu_{12}^0 \nu_{21}^0} & \frac{E_2^0 \nu_{12}^0}{1-\nu_{12}^0 \nu_{21}^0} & 0 \\ \frac{E_2^0 \nu_{12}^0}{1-\nu_{12}^0 \nu_{21}^0} & \frac{E_1^0}{1-\nu_{12}^0 \nu_{21}^0} & 0 \\ 0 & 0 & G_{12}^0 \end{bmatrix}; R = \begin{bmatrix} 1 & 0 & 0 \\ 0 & 1 & 0 \\ 0 & 0 & 2 \end{bmatrix} \quad (5)$$

$Q_k^0$  represents the stiffness of a healthy lamina  $k$  in the absence of matrix cracks.  $E_1^0, E_2^0, \nu_{12}^0, \nu_{21}^0$  and  $G_{12}^0$  represent the elastic moduli for the undamaged lamina. The stiffness of a cracked lamina is given by

$$Q_k^D = - \begin{bmatrix} \frac{E_1^0 \nu_{12}^0 \nu_{21}^0}{(1-\nu_{12}^0 \nu_{21}^0)^2} & \frac{E_1^0 \nu_{12}^0}{(1-\nu_{12}^0 \nu_{21}^0)^2} & 0 \\ \frac{E_1^0 \nu_{12}^0}{(1-\nu_{12}^0 \nu_{21}^0)^2} & \frac{E_2^0}{(1-\nu_{12}^0 \nu_{21}^0)^2} & 0 \\ 0 & 0 & g G_{12}^0 \end{bmatrix} \quad (6)$$

In Eq. (3),  $w_k$  is the damage parameter that is related to the non-dimensionalized crack density  $\delta_k$  for the  $k$ th lamina. The parameter  $g$  is a layup-dependent constant and will depend upon the laminate material as well as the layup sequence. It is defined as the ratio of relative changes in the in-plane shear modulus and the transverse modulus, as a result of damage and is given by

$$g = \frac{\frac{G_{12} - G_{12}^0}{G_{12}^0}}{\frac{E_2 - E_2^0}{E_2^0}} \quad (7)$$

The relationship between the damage parameter ( $w = 1 - (E_2/E_2^0)$ ) of a cracked lamina and the crack density  $\delta$  is established using the micromechanical cracked laminate analysis. A function as shown below relates the damage parameter and the non-dimensionalized crack density.

$$w_k = 1 - \exp(-p)\delta_k \quad (8)$$

where,  $p$  is a constant to be determined either from experiments or computational micromechanics.

In order to capture the damage parameter ( $w_k$ ) and determine its correct value, three dimensional finite element analysis, as a micromechanical tool, is used. The micromechanical cracked laminate modeling approach is based on the computational micromechanics technique. It is used to determine the numerical value of the damage parameter corresponding to each damage mode for a specific laminate; the sole aim of the three dimensional analysis being to capture the constraining effects of the adjacent plies on a cracked ply of interest. The finite element analysis used here employs periodic boundary conditions (PBC) to mimic the behavior for the entire laminate.

To conduct the computational simulations corresponding to each laminate configuration a micromechanical FE model, containing sub-critical ply cracks, is generated. For a particular crack containing laminate, an appropriate RVE representing the material properties, ply specific geometry, and the orientation of the cracks for the given damage state needs to be defined. Furthermore, to invoke the PBCs, the RVE needs to be a repeating unit cell (RUC), which can be a difficult task, but not impossible.

Once the RUC for a crack containing laminate is defined, its geometry can successfully be created by using a suitable FE package such as ANSYS. To implement the model for various crack den-

sities and damage states, a number of three-dimensional FE models are created using ANSYS-APDL environment. It must be remembered that a three-dimensional analysis is required to capture the constraining effects between adjacent plies and the out-of-plane deformation behavior.

To evaluate the effective properties of a lamina, three FE simulations are conducted corresponding to applied strains along (i)  $\epsilon_{11}$ ; (ii)  $\epsilon_{22}$ ; and (iii)  $\epsilon_{12}$ . For each simulation the stresses and strains from the RUC are averaged upon the volume of the element, and are calculated by considering the individual element stresses,  $\sigma_{ij}$ , and strains,  $\epsilon_{ij}$ , as well as the RUC total volume,  $V$ . Thus, the average stress and strain components are given by,

$$\bar{\sigma}_{ij} = \frac{1}{V} \int_V \sigma_{ij} dV \quad (9)$$

$$\bar{\epsilon}_{ij} = \frac{1}{V} \int_V \epsilon_{ij} dV \quad (10)$$

For the homogeneous composite material, the relationship between average stress and average strain is

$$\bar{\sigma}_{ij} = C_{ijkl} \bar{\epsilon}_{kl} \quad (11)$$

The components of the stiffness tensor  $\mathbf{C}$  are determined using Eq. (11) from the volume averaged stresses and strains determined from the three sets of FE simulations described above.

From the components of the stiffness tensor obtained above, the material engineering moduli for a damaged laminate can be obtained by the following relationships.

$$\begin{aligned} E_1 &= \frac{C_{11}C_{22} - C_{12}^2}{C_{22}} \\ E_2 &= \frac{C_{11}C_{22} - C_{12}^2}{C_{11}} \\ G_{12} &= C_{66} \end{aligned} \quad (12)$$

In Eq. (12), terms of the fourth order stiffness tensor are expressed in Voigt notation. The process is repeated for ply cracks in each orientation for the particular laminate. Using this approach it is possible to obtain the evolution of the damage parameter with respect to the crack density. This evolution form is used to determine the constant  $p$  from curve fitting. The value of  $p$  is not unique but is dependent on material and layup sequence used in a laminate. Numerical results from the computational micromechanics approach used to determine the value of  $p$  are given in Section 3.

Following the procedure described above, the effect of matrix cracks can be accounted in any structural level model through the constitutive relation of individual plies. On the other hand, interlaminar cracks or delaminations do not directly affect the individual ply properties. It is known to affect at the scale of a structure. For the problem at hand, it should affect the cross-sectional stiffness properties of the strip. Next section describes the general process of including delamination in a composite strip within the VAM framework based on the sublaminates approach.

### 3. Cross-sectional analysis of a delaminated anisotropic pretwisted strip

A 1D model for a thin pretwisted anisotropic strip in the presence of delamination (Fig. 2) is developed in this section. The 1D model for the strip is obtained by dimensionally reducing the 3D problem into a nonlinear cross-sectional analysis and a nonlinear problem along its longitudinal axis. This is possible in structures where one or more of the geometrical feature of the strip is sufficiently small compared to the other. The small parameters relevant to the strip under consideration are: (i) width to length ratio ( $\delta_b = b/l$ ); (ii) thickness to width ratio ( $\delta_h = h/b$ ); and (iii) the

width times pretwist per unit length ( $\delta_t = bk_1$ ). VAM procedure involves the representation of the strain energy of the strip in terms of the small parameters. This allows for a systematic order analysis of the strain energy functional. In the asymptotic process the strain energy functional is approximated by successively neglecting the higher order terms, whose contribution to the overall energy is relatively negligible. This process is carried out until difference in stationary points, i.e. kinematic field variables, corresponding to successive asymptotic steps are negligible in an asymptotic sense. The model development, in this work, is limited to strips with Winckler layup for the ease of enumeration of the methodology and determination of closed form analytical solutions. A brief summary of the key steps involved in the mathematical formulation is described here.

Distinction should be made between the delaminated and the healthy part of the strip during the development of the kinematics. This is achieved by following the sublaminates approach. Regions above and below the delamination are represented by superscript 1 and 2, respectively. The 3-D kinematics of the pretwisted strip is developed following the procedure enumerated by Danielson and Hodges [61] and directly adapted from Hodges et al. [53] and Guruprasad et al. [57]. The 3-D strains expressed in terms of the 2-D mid-surface strains and curvatures by following the relation:  $\Gamma_{\alpha\beta}^{(1,2)} = \epsilon_{\alpha\beta}^{(1,2)} + (x_3 \pm \frac{h}{4})\rho_{\alpha\beta}^{(1,2)}$ . Here,  $\epsilon_{\alpha\beta}^{(1,2)}$  are the mid-surface membrane strains and  $\rho_{\alpha\beta}^{(1,2)}$  are the middle surface bending curvatures of the top and bottom sublaminates. Explicit expressions for the first order 2-D strains and curvatures are determined to be:

$$\epsilon_{11}^{(1,2)} \approx \gamma_{11} - x_2 \kappa_3 + k_1 x_2^2 \kappa_1 + \frac{x_2^2 \kappa_1^2}{2} + w_3^{(1,2)} \kappa_2$$

$$\epsilon_{22}^{(1,2)} \approx w_{2,2}^{(1,2)} + \frac{1}{2} w_{3,2}^{(1,2)2}$$

$$2\epsilon_{12}^{(1,2)} \approx w_{1,2}^{(1,2)} + k_1 (x_2 w_{3,2}^{(1,2)} - w_3^{(1,2)}) + k_1 (x_2 w_{3,2}^{(1,2)} - w_3^{(1,2)})$$

while the curvatures are,

$$\rho_{11}^{(1,2)} \approx \kappa_2$$

$$\rho_{22}^{(1,2)} \approx -w_{3,22}^{(1,2)}$$

$$2\rho_{12}^{(1,2)} \approx -2\kappa_1$$

(13)

The 2-D strains and curvatures in Eq. (13) contain both linear and non-linear terms. Nonlinear terms arising due to moderate local rotations are highlighted with an underline. In Eq. (13),  $\gamma_{11}$  and  $\kappa_i$ 's are the 1-D strain measures and  $w_i$ 's are the warping displacements. Where necessary, the delaminated and undamaged/healthy regions of the laminate will be identified in the equations by superscript ( $d$ ) and ( $h$ ).

The 2-D strains and curvatures are grouped as  $\epsilon^{(1,2)} = [\epsilon_{11}^{(1,2)} \epsilon_{22}^{(1,2)} \underline{2\epsilon_{12}^{(1,2)}} \rho_{11}^{(1,2)} \rho_{22}^{(1,2)} \underline{2\rho_{12}^{(1,2)}}]$ .

The laminate stiffness matrix of the healthy part of the cross-section is given by

$$K^h = \begin{bmatrix} A^h & B^h \\ B^h & D^h \end{bmatrix} \quad (14)$$

and that of the delaminated sublaminates is given by

$$K^d = \begin{bmatrix} A^d & 0 \\ 0 & D^d \end{bmatrix} \quad (15)$$

It should be noted that since Winckler layup is considered the sublaminates above and below the delamination contain symmetric laminate layup sequence. The stiffness terms used above are defined as

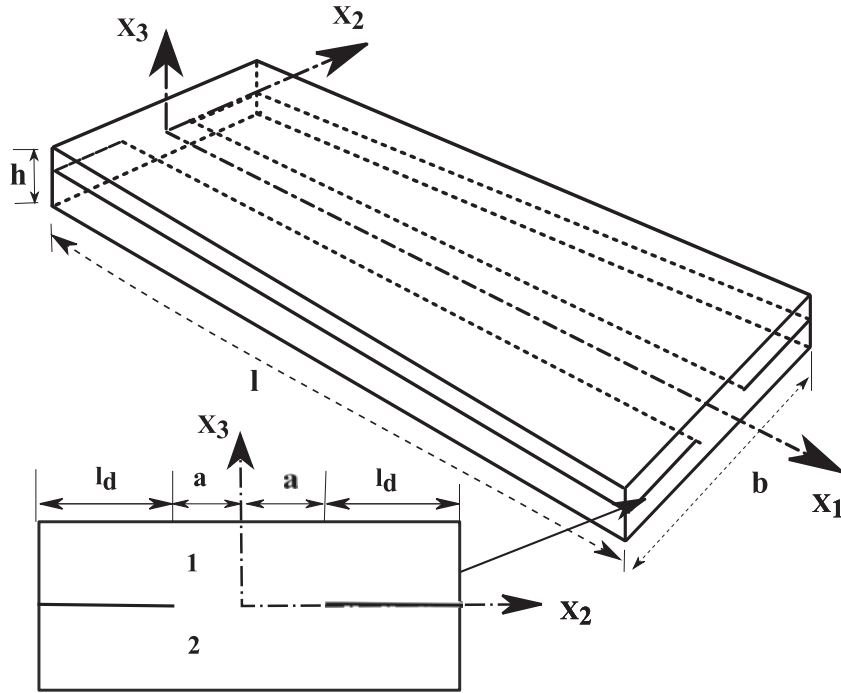


Fig. 2. The strip model shows geometry and coordinate system. The cross-sectional view of edge delamination is highlighted.

$$(A_{ij}^h, B_{ij}^h, D_{ij}^h) = \int_{-h/2}^{h/2} (\bar{Q}_{ij}, \bar{Q}_{ij}z, \bar{Q}_{ij}z^2) dz \quad (16)$$

$$(A_{ij}^d, D_{ij}^d) = \int_{-h/4}^{h/4} (\bar{Q}_{ij}, \bar{Q}_{ij}z^2) dz \quad (17)$$

The 2D strain energy density of the strip is determined as,

$$U_{1D} = \int_{-b/2}^{-a} \epsilon^{(1)\top} K^d \epsilon^{(1)} dx_2 + \int_{-a}^a \epsilon^{(1)\top} K^h \epsilon^{(1)} dx_2 + \int_a^{b/2} \epsilon^{(1)\top} K^d \epsilon^{(1)} dx_2 + \int_{-b/2}^{-a} \epsilon^{(2)\top} K^d \epsilon^{(2)} dx_2 + \int_{-a}^a \epsilon^{(2)\top} K^h \epsilon^{(2)} dx_2 + \int_a^{b/2} \epsilon^{(2)\top} K^d \epsilon^{(2)} dx_2 \quad (18)$$

where,  $\epsilon_{ab}$  and  $\rho_{ab}$  are the strains and curvatures as defined in Eq. (13), 'a' is the location of the delamination from the origin as shown in the Fig. 2. Total delamination size along the  $x_2$  direction is  $2l_d$ , where  $l_d = (b/2) - a$ .

The strain energy functional is extremized with respect to the field variables - warpings. The final form of the governing differential equations obtained can be presented in terms of the generalized forces and moments, corresponding to the healthy and damaged part of the strip, as below

$$\begin{aligned} N_{22}^{(1,2)(d)} &= 0 \\ N_{12}^{(1,2)(d)} &= 0 \\ M_{22}^{(1,2)(d)} &= 0 \end{aligned} \quad (19)$$

$$\begin{aligned} N_{12}^{(1)(h)} + N_{12}^{(2)(h)} &= 0 \\ N_{22}^{(1)(h)} + N_{22}^{(2)(h)} &= 0 \\ M_{22}^{(1,2)(h)} \pm \frac{h}{4} N_{22}^{(1,2)(h)} &= 0 \end{aligned} \quad (20)$$

It was observed that the governing equilibrium equations have a form similar to the expressions obtained by Makeev et al. [59].

For healthy strip, without any delamination, the above set of equilibrium equations reduce to

$$N_{12}^h = 0, \quad N_{22}^h = 0, \quad M_{22}^h = 0 \quad (21)$$

Minimization of the strain energy density also gives rise to a set of natural and essential boundary conditions, apart from the governing equations. These boundary conditions needs to be enforced on the general solution of the warping obtained after solving Eq. (20). In addition to these boundary conditions, global constraints arising from the definitions of warpings and local rotations, and interface boundary condition, necessary to ensure continuity of warpings across the sublaminates in the healthy region of the strip has to be enforced. Mathematically these constraints and interface conditions take the following form,

$$\begin{aligned} \int_{-b/2}^{-a} w_i^{1d} dx_2 + \int_{-a}^a w_i^h dx_2 + \int_a^{b/2} w_i^{1d} dx_2 \\ + \int_{-b/2}^{-a} w_i^{2d} dx_2 + \int_a^{b/2} w_i^{2d} dx_2 = 0 \\ \int_{-b/2}^{-a} w_{3,2}^{1d} dx_2 + \int_{-a}^a w_{3,2}^h dx_2 + \int_a^{b/2} w_{3,2}^{1d} dx_2 \\ + \int_{-b/2}^{-a} w_{3,2}^{2d} dx_2 + \int_a^{b/2} w_{3,2}^{2d} dx_2 = 0 \end{aligned} \quad (22)$$

$$\begin{aligned} w_i^{1h} &= w_i^{2h} \\ w_{3,2}^{1h} &= w_{3,2}^{2h} \end{aligned} \quad (23)$$

Solution to the unknown warpings are determined by solving the Euler-Lagrange differential equations given in Eq. (20), subject to the essential and natural boundary conditions and the additional constraints given in Eq. (23). Following the determination of the warping terms, the strip strain energy,  $U_{1D}$ , is obtained by integrating the expression in Eq. (18). The 1-D strain energy,  $U_{1D}$ , is expressed in terms of the linear and nonlinear 1D strain measures as,

$$U_{1D} = \frac{1}{2} \epsilon_L^T [S_L] \epsilon_L + \epsilon_L^T [S_{LN}] \epsilon_N + \frac{1}{2} \epsilon_N^T [S_N] \epsilon_N \quad (24)$$

where the linear and nonlinear 1D strain measures,  $\epsilon_L$  and  $\epsilon_N$  respectively are defined as follows:

$$\epsilon_L = \{\gamma_{11}, \kappa_1, \kappa_2, \kappa_3\}^T$$

$$\epsilon_N = \{\kappa_1^2, \kappa_2^2, \kappa_2 \gamma_{11}, \kappa_2 \kappa_3, \kappa_2 \kappa_1\}^T$$

and the matrices  $[S_L]$ ,  $[S_{LN}]$ , and  $[S_N]$  are partitions of a  $9 \times 9$  matrix  $[S]$  representing the linear and nonlinear stiffness part and are given in [Appendices A and B](#). For a healthy strip, stiffness terms are obtained by substituting the length of the delamination  $l_d = 0$  i.e by substituting  $a = \frac{b}{2}$ .

Linear extension-twist coupling is reflected in  $S_{12}$ , while trapeze effect, which is a nonlinear extension twist coupling exhibited through  $S_{15}$  is captured in terms of delamination parameter, ‘a’. Other nonlinearities like the purely torsional nonlinearity ( $S_{25}$  and  $S_{55}$ ) and nonlinear bending-twist coupling

( $S_{35}, S_{26}, S_{59}, S_{69}$  &  $S_{99}$ ) have also been captured asymptotically in terms of delamination parameter. The process described is general, however, for the purpose of demonstrating its utility on the trapeze effect closed form solutions of the stiffness terms are derived for a delaminated strip with antisymmetric layup. It should be noted that since these 1D stiffness terms are determined in terms of ply level stiffnesses, effect of matrix cracks on any layer can be naturally accounted for, in addition to delamination, by following the methodology presented in Section 2.

The framework developed above is used to capture the trapeze effect in the strip. The total strain energy of the strip is given as

$$U = \int_0^l U_{1D}(\gamma_{11}, \kappa_1, \kappa_2, \kappa_3) dx_1 \quad (25)$$

The principle of virtual work for an axially loaded strip can be written as

$$\delta U = F_1 \delta u_1(l) \quad (26)$$

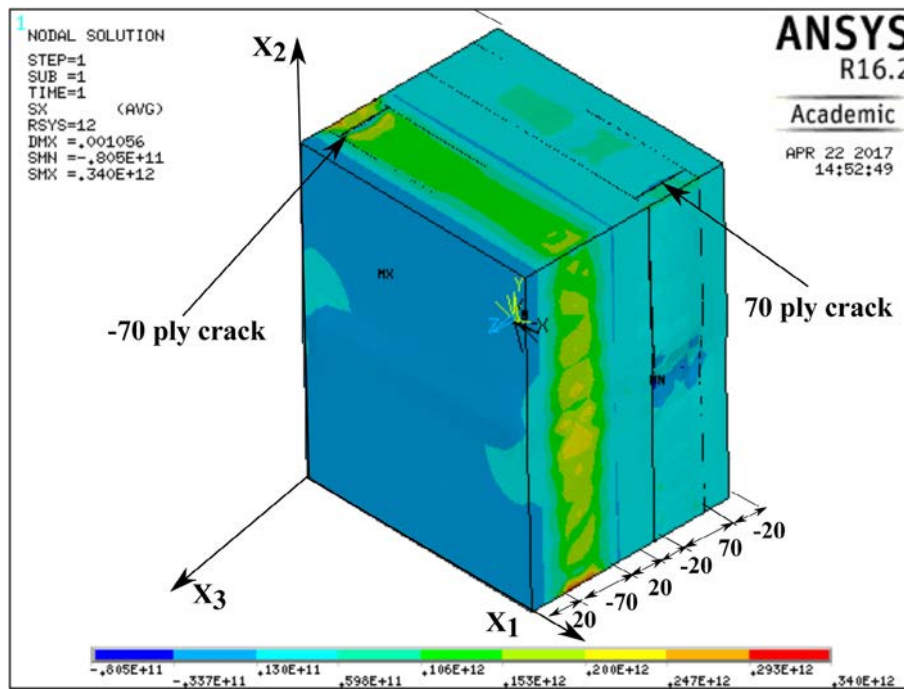


Fig. 3. Finite element model of RUC for a  $[20_2/(-70)_4/20_2/-20_2/(70)_4/-20_2]_T$  laminate containing cracks in the  $\pm 70^\circ$  plies.

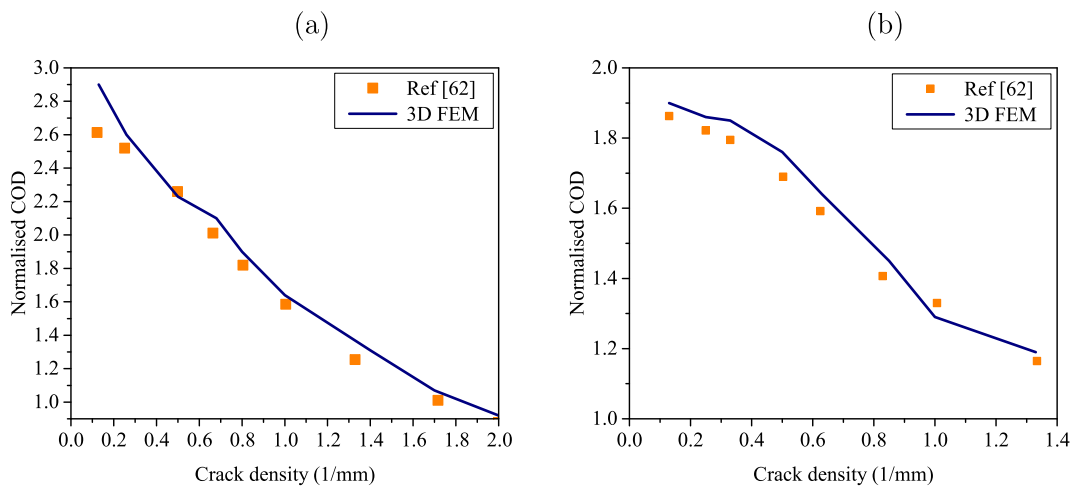


Fig. 4. Validation of variation of normalized COD with crack density for (a)  $[0/90]_s$  and (b)  $[0/90/-45/45]_s$  laminates.

where,  $F_1$  is the axial force. For the case of antisymmetric layup under an axial force, both  $\kappa_2$  and  $\kappa_3$  are zero. The two governing equilibrium equations thus reduce to algebraic equations for the coupled extension-twist problem:

$$\frac{\partial U_{1D}}{\partial \gamma_{11}} = F_1 \tag{27}$$

$$\frac{\partial U_{1D}}{\partial \kappa_2} = 0 \tag{28}$$

These equations are solved by using the first equation to eliminate  $\gamma_{11}$  in favor of  $F_1$  and then using the second to express  $F_1$  in terms of  $\kappa_1$ . Here  $k_1$  and  $\kappa_1$  are constant so that the tip pretwist angle can be written as  $\theta_0 = lk_1$  and the elastic tip twist angle  $\theta = l\kappa_1$ . The results can be written in terms of stiffness terms.

$$F_1 = \left\{ \frac{\theta \left( l^2 (S_{12}^2 - S_{11}S_{22}) + 3\theta l (S_{12}S_{15} - S_{11}S_{25}) + 2\theta^2 (S_{15}^2 - S_{11}S_{55}) \right)}{l^2 (S_{12} + 2\theta S_{15})} \right\} \tag{29}$$

### 4. Results and discussion

#### 4.1. Characterization of matrix cracked laminates

In this section numerical results from computational micromechanics simulations are shown and the values of the constant  $p$

determined from the analysis are presented for various layup sequences. The values of the constant  $p$  determined from the micromechanics analysis are subsequently used in ply level stiffness degradation model to calculate strip stiffness degradation. Effect of strip stiffness degradation due to matrix cracks on the trapeze effect are then highlighted. Validation of the VAM based strip model accounting for delamination is done by quantitatively comparing trapeze effect predictions with experimental results. Finally, effect of both matrix and delamination on the trapeze effect is discussed.

The capability of the FE based micromechanics approach to capture the effect of matrix cracks on ply level stiffness degradation is first demonstrated. This is undertaken by modeling RUC of laminates containing matrix cracks of various crack densities and different damage states using the ANSYS-APDL environment. In all the models plies are finely meshed using 20-node SOLID186 brick elements. The aspect ratio of the elements considered in the models are close to one. It is necessary to ensure proper displacement of cracked surfaces during deformation. This is achieved by not

**Table 1**  
Material properties.

Materials	$E_{11}$ (GPa)	$E_{22}$ (GPa)	$G_{12}/G_{13}$ (GPa)	$\nu_{12}$
Glass/epoxy	46.2	12	5	0.3
Graphite/epoxy	144.7	9.5	4.7	0.31
Carbon/epoxy	127.8	9.4	4.2	0.28
Graphite/cyanate	135.6	9.9	4.2	0.3

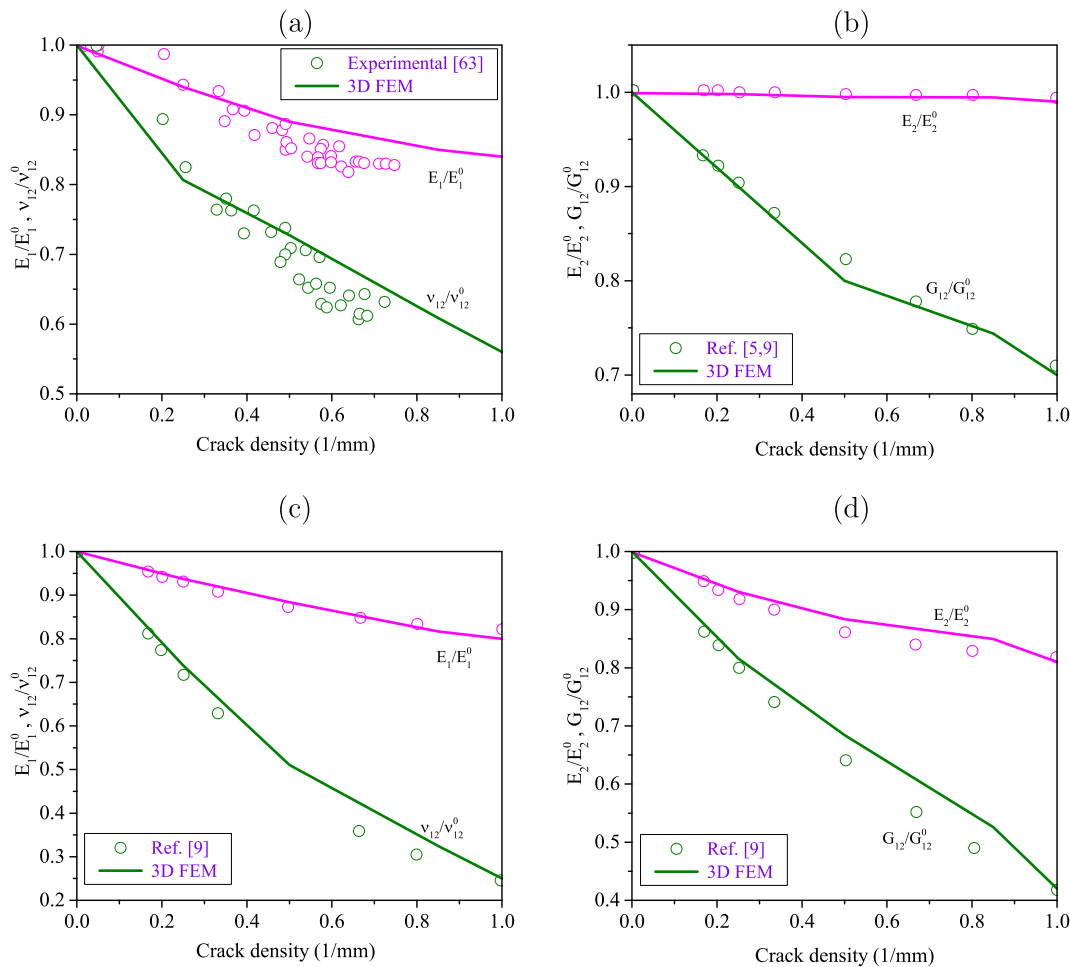


**Fig. 5.** The normalised engineering moduli of  $[0/90]_s$  laminate for damage state 1 ((a) and (b)) and for damage state 2 ((c) and (d)) of glass/epoxy material.

connecting nodes along cracked surfaces with each other. Delamination is not considered in RUCs; hence, nodes along adjacent ply interfaces are merged to ensure continuity of displacements. Further, PBCs should account for continuity between the RUC surface. For the in-plane response, PBCs should be applied on the opposing faces of the RUC, which involves the imposition of displacement constraints between the node pairs and is accomplished in ANSYS by defining appropriate constraint equations. In symmetric laminates, symmetric boundary condition is added to the face of the RUC that corresponds to the laminate mid-plane due to the presence of mid-plane symmetry. A representative FE model of RUC simulated in ANSYS is shown in Fig. 3. This RUC corresponds to a Winckler layup  $[(\alpha)_2/(\alpha - 90)_4/(\alpha)_2/-(\alpha)_2/(90 - \alpha)_4/-(\alpha)_2]_T$ , with  $\alpha = 20^\circ$ . Matrix cracks are considered to be present in the  $(\alpha - 90)_4$  and  $(90 - \alpha)_4$  plies. The procedure is validated by determining the COD variation for different crack densities in  $[0/90]_s$  and  $[0/90/-45/45]$  glass-epoxy composite. Fig. 4 shows that COD decreases with increase in crack density, which is due to the relieving of the tensile stress fields between adjacent cracks. To gain confidence in the 3D FEM procedure adopted, the simulation results are validated against experimental results for predicting COD for different crack densities. The simulation results show good agreement with the data reported in [62].

A large body of experimental and analytical results [63,11,64,65] of stiffness degradation in cross-ply laminates are reported in the literature. Hence, for the purpose of validation,  $[0/90]_s$  laminates containing two different damage states are first considered - referred here as damage state 1 and damage state 2.

Damage state 1 corresponds to the case when matrix cracks are present only in the  $90^\circ$  plies and damage state 2 corresponds to the case when cracks are present in the  $0^\circ$  and the  $90^\circ$  plies. Fig. 5 shows degradation in modulus (longitudinal and transverse), shear modulus and Poisson's ratio with crack density evolution in the laminate. These material properties for the damaged laminate was determined by using their appropriate definitions in terms of volume averaged stresses and strains. Predictions of the damage state 1 are shown in the Fig. 5a and b and damage state 2 are shown in Fig. 5c and d. It is observed that FE based computational micromechanics approach is able to capture the material property degradation of the laminate quantitatively.

The procedure described above is used to establish the relation between damage parameter and cracked density in plies. For this purpose, simulations were carried out for: (a)  $[0/90]_s$  and  $[0/90_5/0]_T$  carbon/epoxy laminates; (b)  $[0/90_3]_s$  and  $[0/90]_s$  glass/epoxy laminates; (c)  $[0/90_3]_s, [0/90_2]_s, [0_2/90_2]_s$  and  $[0/90]_s$  graphite/epoxy laminates; and (d)  $[\alpha_2/(\alpha - 90)_4/\alpha_2/-(\alpha)_2/(90 - \alpha)_4/-(\alpha)_2]_T$  with  $\alpha = 20^\circ$  for glass/epoxy and graphite/cyanate laminates. Material properties used in the simulations are reported in the Table 1. In all the simulations cracks were considered to be present only in the  $90^\circ$  plies. The effective  $E_2$  is determined from the simulations and the damage parameter is calculated. Fig. 6a–d shows the calculated damage parameter versus crack density for all the simulated cases. Relation between damage parameter and crack density, given in Eq. (8), is used to fit the data in Fig. 6 to determine the value of constant 'p' in all the cases. The calculations highlight that value of 'p' is material

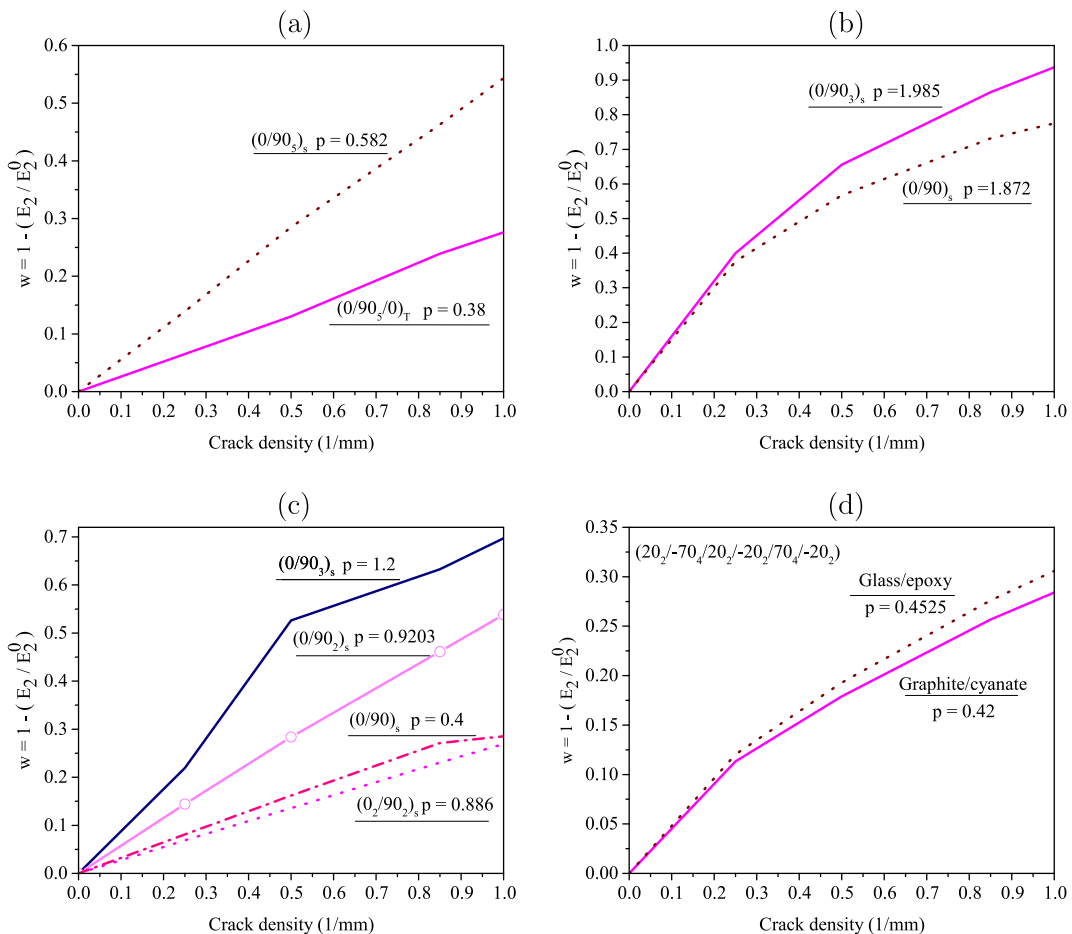


Fig. 6. Damage constant v/s crack density for (a) carbon/epoxy, (b) glass/epoxy, (c) graphite/epoxy, and (d) antisymmetric layup with different stacking sequence. The value of p by using the curve fitting method for different stacking sequence.

and lay-up dependent; values corresponding to different lay-up sequences used in laminates are given in Fig. 6 and tabulated in Table 3.

4.2. Model predictions and validation

In Fig. 7 VAM based model predictions of the degradation of the longitudinal stiffness and the shear modulus of all the cross-ply laminates for which the constant ‘p’ was determined is presented. Additionally, results from FEM, obtained during the computational micromechanics analysis, and experimental results are shown for the purpose of validation. Cross-sectional stiffness terms for healthy strip are provided in Appendix A; if these stiffness terms are determined by accounting for matrix cracks then they can be used to calculate the strip effective properties. Matrix cracks in strip can be accounted by including damage parameter while determining the individual ply stiffness terms (see Eqs. (6) and (16)) as described in Section 3. By considering only unit axial load and unit moment along  $x_1$ , longitudinal stiffness and shear modulus of the strip are determined, respectively. Model predictions bring out all the salient features typically observed in cracked ply-laminates. It was observed that there is progressive degradation of the longitudinal stiffness with evolution of the crack density. Further, stiffness degradation rate is observed to be function of net 90° ply thickness within the laminate and material. The degradation rate increases with increase in 90° ply thickness within the strip. It was also observed that stiffness reduction in glass-fiber strip was higher than carbon-fiber strips; this is due

**Table 2**  
Geometric properties.

Length (m)	Width (m)	Thickness (m)	Pretwist (degree/m)
0.254	0.026	0.0012	2

to the significantly higher load carried by transverse plies in glass-fiber strips due to the high mismatch in its modulus along longitudinal and transverse direction.

Following the micromechanical characterization of the matrix cracked laminates, its effect on trapeze effect is investigated. For this purpose, cantilevered strips made of graphite/cyanate and glass/epoxy are considered with Winckler layup corresponding to  $\alpha = 20$  and  $\alpha = 30$ . Material properties and geometry of the strips used in the analysis are given in Table 1, 2 respectively. Axial force is applied at the free end of the cantilevered strips. Fig. 8a and b shows the variation of the end-twist as a function of axial force in graphite/cyanate and glass/epoxy strip, respectively. Matrix cracks are considered to be in the  $(\alpha - 90)_4$  and  $(90 - \alpha)_4$  set of plies. Model predictions for both set of strips are shown for three different cases of crack density: (i)  $\rho = 0$  cr/mm (healthy strip); (ii)  $\rho = 1$  cr/mm and (iii)  $\rho = 2$  cr/mm. Experimental results corresponding to the healthy graphite/cyanate strip are taken from [59]. The present theory is able to predict the nonlinear extension-twist response of the healthy strips and for the graphite/cyanate case the model predictions are in agreement with the experimental observations. It was observed that for a given axial load the resultant

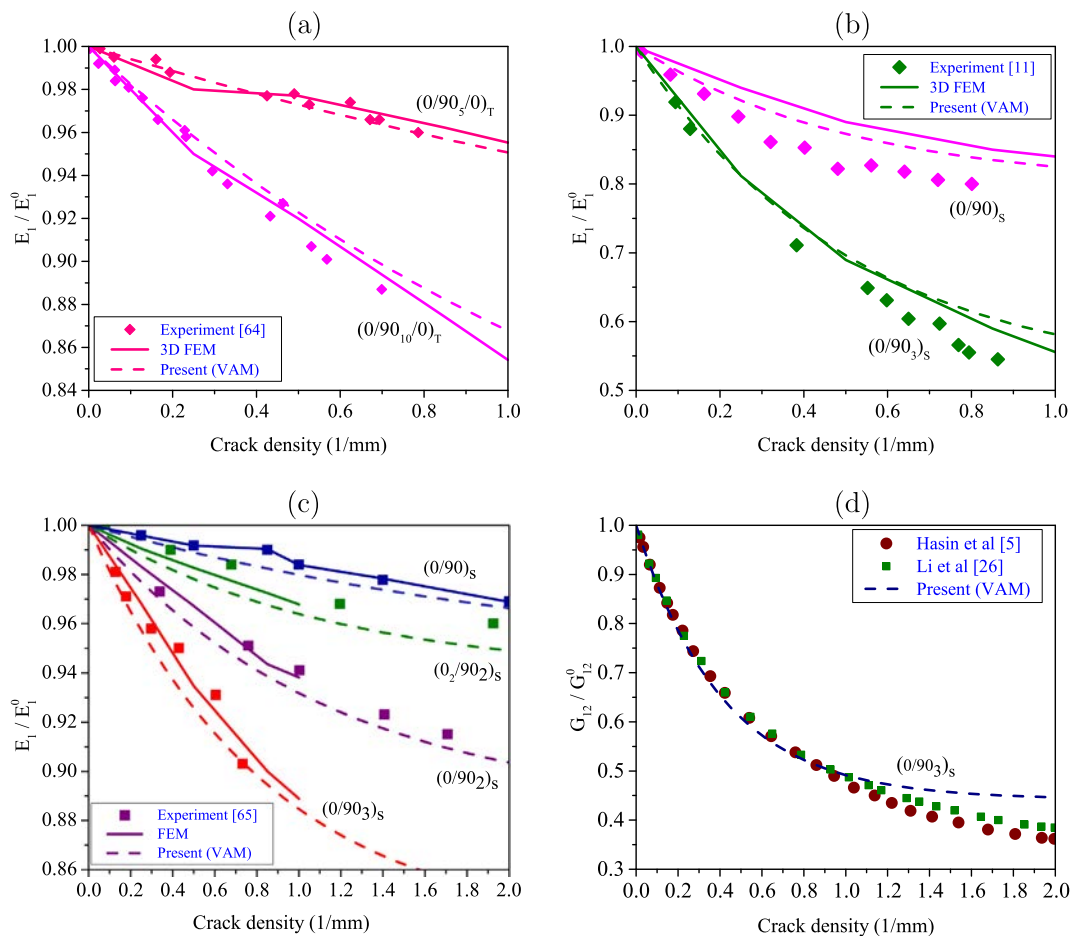


**Fig. 7.** Validation of present and FE model with experimental result for normalised effective axial stiffness of (a) carbon/epoxy, (b) glass/epoxy, and (c) graphite/epoxy and (d) shear modulus of glass/epoxy for different layup orientation.

end-twist, in both sets of strips, increased with increase in matrix crack density. The increase in matrix crack density leads to reduction in the nonlinearity of the end-twist to axial force relationship.

Effect of delamination on the trapeze effect in graphite/cyanate and glass/epoxy strips are shown in Fig. 9. Model predictions are presented for healthy strips, strips with 50% and 75% edge delamination. Material properties and geometry of the strips used in the analysis are given in Table 1 and 2 respectively. Fig. 9 shows the comparison of end-twist predictions from the model with experi-

mental data from Makeev and Armanios [59] and Armanios and Makeev [60]. The comparison has been done for three different cases, viz., Fig. 9(a) graphite/cyanate  $\alpha = 20^\circ$  (b) graphite/cyanate  $\alpha = 30^\circ$  (c) glass/epoxy  $\alpha = 20^\circ$ . Model and experiments show non-linear behavior between the applied axial force and the resultant end-twist. The presence of edge delamination leads to reduction in the axial-twist coupling. In general, the model predictions are in good agreement with experimental observations. The variation of end twist with delamination for graphite/cyanate and glass/

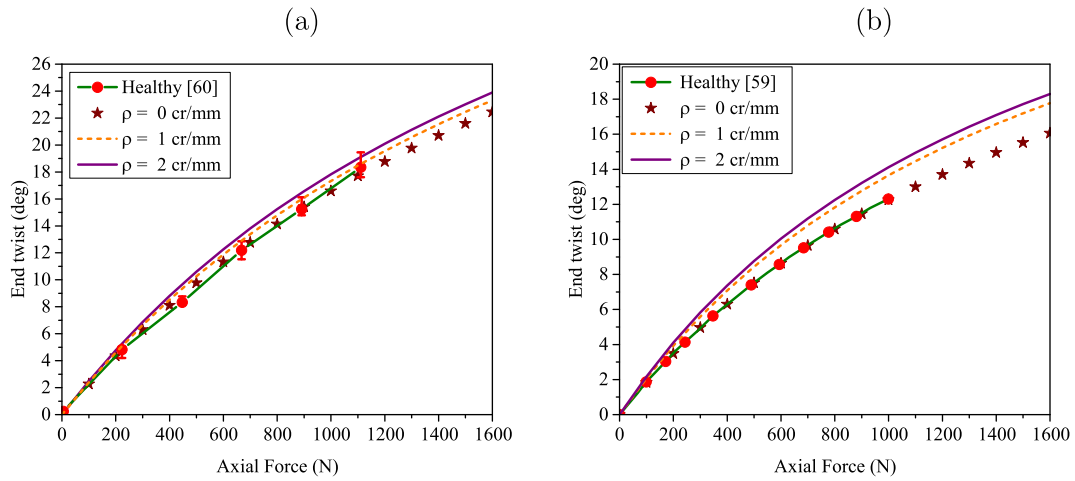


Fig. 8. Influence of axial force on the extension-twist coupling ( $\alpha = 20^\circ$ ) with matrix crack density ( $\rho$ ) on (a) graphite/cyanate and (b) glass/epoxy materials.

Table 3  
The values of p and g.

Materials	Layup	p	g (crack/mm)			
			0.25	0.5	0.85	1
Glass/epoxy	[0/90] <sub>s</sub>	1.985	0.62	0.64	0.69	0.72
	[0/90 <sub>3</sub> ] <sub>s</sub>	1.875	0.64	0.68	0.72	0.74
	[20 <sub>2</sub> /-70 <sub>4</sub> /20 <sub>2</sub> /-20 <sub>2</sub> /70 <sub>4</sub> /-20 <sub>2</sub> ]	0.42	0.39	0.42	0.46	0.46
Graphite/epoxy	[0/90] <sub>s</sub>	0.39	0.73	0.70	0.68	0.70
	[0/90 <sub>3</sub> ] <sub>s</sub>	1.2	0.76	0.71	0.69	0.70
	[0/90 <sub>2</sub> ] <sub>s</sub>	0.92	0.70	0.70	0.68	0.68
	[0 <sub>2</sub> /90 <sub>2</sub> ] <sub>s</sub>	0.88	0.75	0.72	0.71	0.72
Carbon/cyanate	[20 <sub>2</sub> /-70 <sub>4</sub> /20 <sub>2</sub> /-20 <sub>2</sub> /70 <sub>4</sub> /-20 <sub>2</sub> ]	0.42	0.38	0.40	0.38	0.39
	[0 <sub>2</sub> /90 <sub>4</sub> /0 <sub>2</sub> /0 <sub>2</sub> /90 <sub>4</sub> /0 <sub>2</sub> ]	0.40	0.60	0.72	0.68	0.67
Carbon/epoxy	[0/90 <sub>5</sub> /0]	0.38	0.80	0.078	0.73	0.74
	[0/90 <sub>5</sub> ] <sub>s</sub>	0.58	0.80	0.80	0.74	0.74

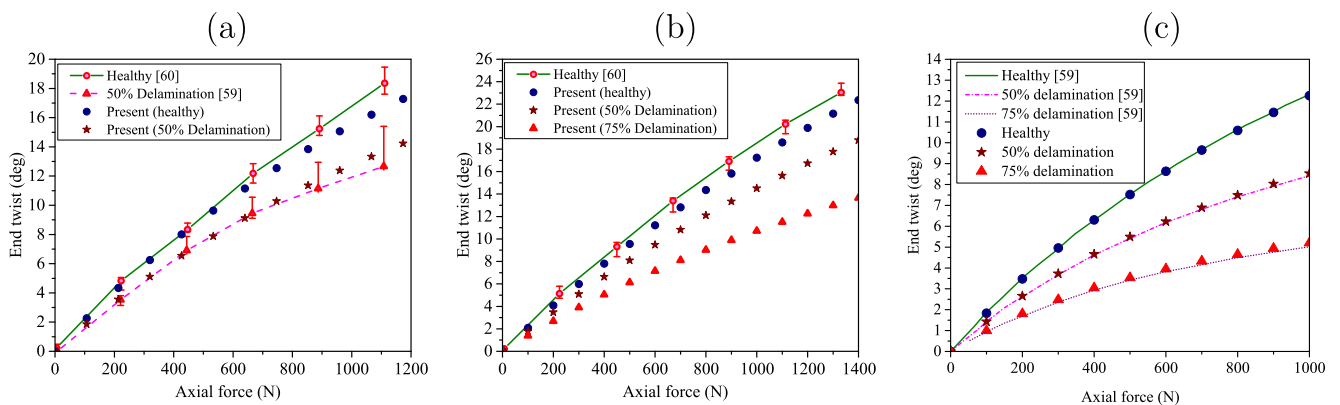


Fig. 9. Comparison of model prediction with experimental data for healthy and delaminated strip of graphite/cyanate material for (a)  $\alpha = 20^\circ$ , (b)  $\alpha = 30^\circ$  and (c) glass/epoxy material  $\alpha = 20^\circ$ .

epoxy material are shown in Fig. 10. It gives information of end twist at an axial force of 1 kN for different ply angle. Analysis of Fig. 10 shows that the extension-twist coupling in strips with ply orientations corresponding to  $\alpha = 0^\circ, 45^\circ$  and  $90^\circ$ , vanishes. The coupling is found to be maximum for  $\alpha = \pm 28^\circ$  for graphite/cyanate and  $\alpha = \pm 26^\circ$  for glass/epoxy strips. These observations agree with the results reported by Makeev et al. [59]. Fig. 11a and b show model predictions of the extension-twist behavior of healthy, matrix cracked, delaminated and strips with matrix cracks and delamination. It was observed that matrix crack enhances the extension-twist coupling; on the contrary, delamination reduces it. Strips having matrix cracks and either 50% or 75% delamination show reduced extension-twist coupling.

4.3. Discussion on strip behavior

Analyses of strips in the presence of matrix cracks and delamination have shown that the two damage modes have completely different effect on their extension-twist behavior. Matrix cracks increases the extension-twist coupling while edge delamination reduces it. Matrix cracks and delamination in the strips causes degradation in their cross-sectional stiffness terms. The most basic effect of intralaminar cracking is reduction in the overall effective material stiffness properties of the laminate. Degradation of mate-

rial stiffness properties lead to reduction in the strip cross-sectional stiffness properties. For our analyses here, the linear and nonlinear stiffness terms,  $S_{12}, S_{22}, S_{25}, S_{55}$  and  $S_{15}$  are considered. These cross-sectional stiffness terms directly affect the extension-twist coupling (see Eq. (29)). The reduction in these properties due to intralaminar cracking is shown in Fig. 12 in graphite/cyanate strip with Winckler layup and typical values of  $\alpha$  ranging from  $0^\circ$  to  $45^\circ$ . The transverse cracks are considered to be in the  $(\alpha - 90)_4$  and  $(90 - \alpha)_4$  set of plies. The properties are normalized with respect to their initial values (healthy). All the strip cross-sectional stiffness properties reduce substantially due to ply cracking. The degradation in properties is severe initially during the damage development (i.e., for low crack densities), and the properties reach their saturation values asymptotically at high crack densities, after which significant changes in stiffness properties are not expected. In particular, cross-sectional stiffness terms  $S_{12}$  and  $S_{25}$  drop almost 70% for the case when  $\alpha = 0^\circ$ ; however, there is negligible change in these stiffness terms for other values of  $\alpha$ . Here, it is worthwhile to note that  $S_{12}$  couples extension-twist and  $S_{25}$  is a measure of nonlinear twist. Since there is no significant drop in these values for non-zero  $\alpha$  values, extension-twist coupling does not drop.

The degradation of the stiffness coefficients with increase in mid-surface delamination length is plotted in Fig. 13 for graphite/

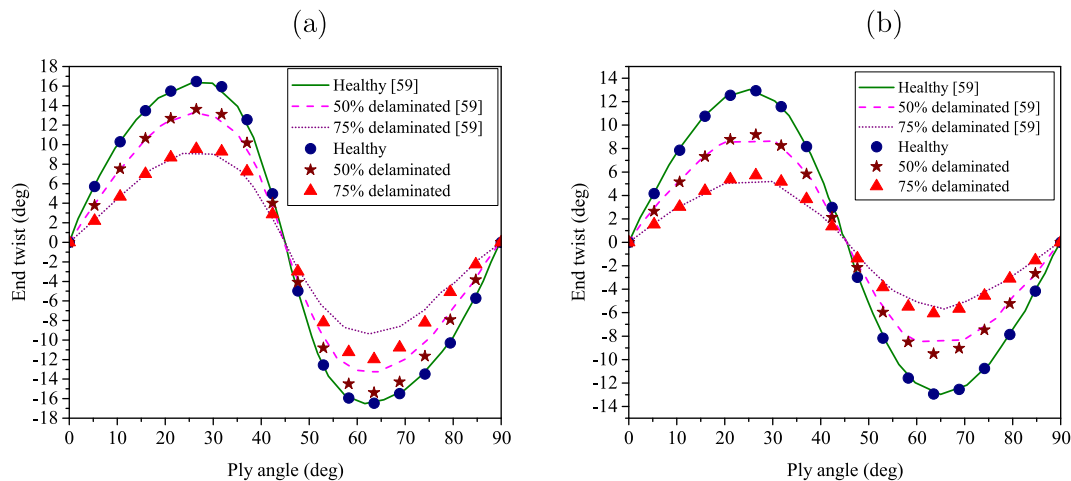


Fig. 10. Influence of delamination on extension-twist coupling for (a) graphite/cyanate and (b) glass/epoxy materials for various ply angle on laminates at 1 kN.

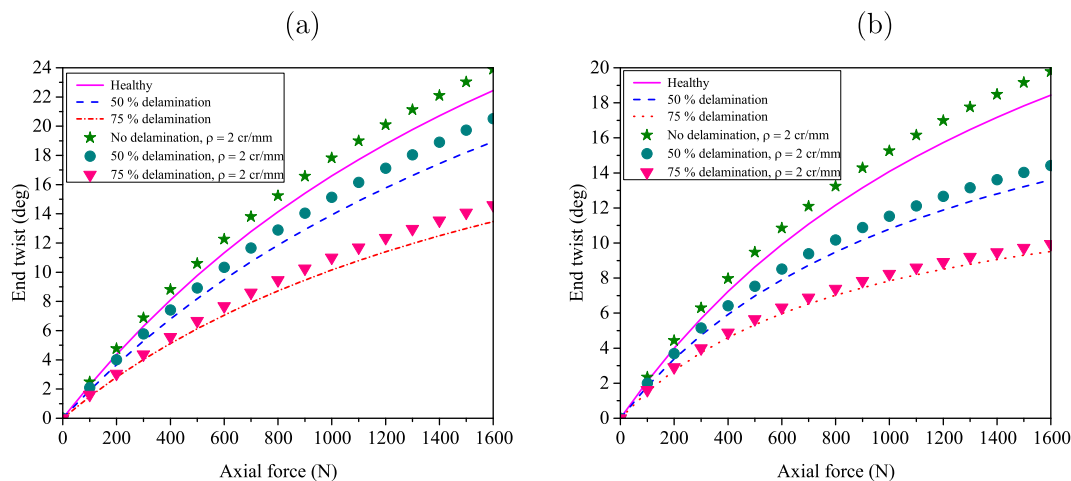
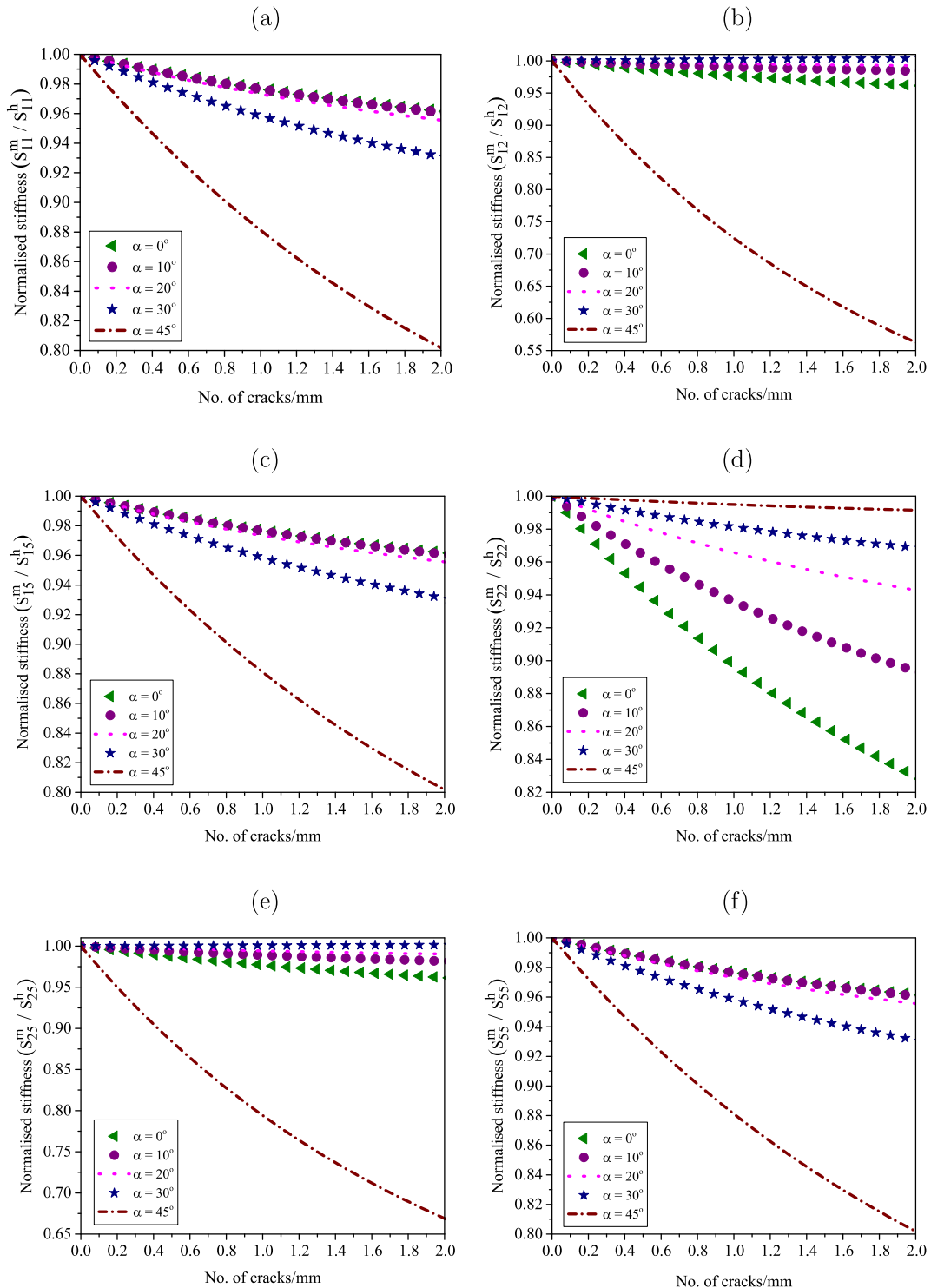


Fig. 11. Influence of axial force on the extension-twist coupling in strips having both delamination and matrix cracks is shown for two different materials: (a) graphite/cyanate and (b) glass/epoxy materials.

cyanate strip having Winckler layup and typical values of  $\alpha$  ranging from  $0^\circ$  to  $45^\circ$ . The properties are normalized with respect to their initial values (healthy). It was observed that delamination length does not have much effect on stiffness coefficients  $S_{11}$  and  $S_{33}$ . Also, the relationship between classical stiffness coefficients and delamination length is linear. This was not the case in strips having only matrix cracks where even classical linear cross-sectional stiffness

terms showed nonlinear relationship with crack density. Linear cross-sectional stiffness term  $S_{12}$  and non-linear term  $S_{25}$  were found to be very sensitive to delamination length (Fig. 13). Again, this observation is in contrast to the behavior of these terms for non-zero  $\alpha$  and  $\alpha = 45^\circ$  values in the case of strips with only matrix cracks. Sharp degradation in  $S_{12}$  and  $S_{25}$  due to mid-surface delamination signifies the reduction in the extension-twist coupling and



**Fig. 12.** Influence of crack density ( $\rho$ ) on normalized extension-twist stiffness terms (b)  $S_{12}$ , (c)  $S_{15}$ , (e)  $S_{25}$ , normalized nonlinear torsional stiffness term (f)  $S_{55}$ , normalized linear torsional stiffness term (d)  $S_{22}$  and normalized extensional term (a)  $S_{11}$  for graphite/cyanate material. The stiffness terms are normalized with respect to stiffness values of a healthy strip.

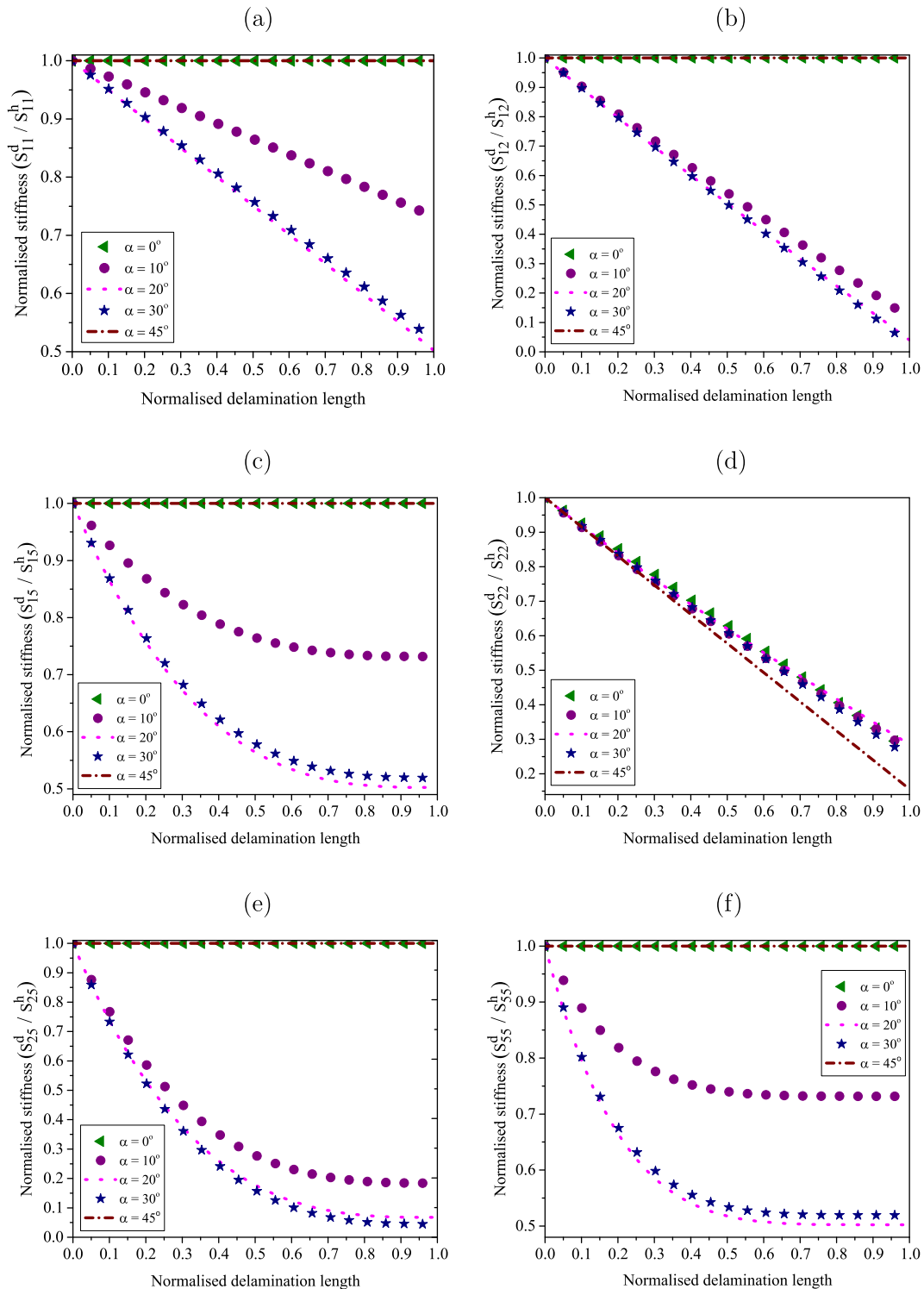


**Fig. 13.** Influence of delamination on normalized extension-twist stiffness terms (b)  $S_{12}$ , (c)  $S_{15}$ , (e)  $S_{25}$ , normalized nonlinear torsional stiffness (f)  $S_{55}$ , normalized linear torsional stiffness terms (d)  $S_{22}$  and normalized extensional term (a)  $S_{11}$  for graphite/cyanate material. The stiffness terms are normalized with respect to stiffness values for a healthy strip.

the nonlinear twist in the strip. In fact, in the absence of pretwist and with 100% delamination, the structure will behave as two strips with symmetric layup leading to zero linear extension-twist coupling and nonlinear twist. This can be readily determined by substituting the total delamination size ( $2l_d = b - a$ ) to be equal to 'b' and pretwist  $k_1$  to be zero. It is, however, inappropriate to generalize the results observed here and claim that delaminations

always lead to reduction in the extension-twist coupling in strips where such a deformation mode is possible. Makeev and Armanios [59] have shown that type of delamination influences the coupling behavior. Their model and experimental data showed less than 0.2% change in end-twist between healthy and 75% internally delaminated strips unlike the significant drop in coupling observed even in 50% edge delaminated strips.

## 5. Conclusions

This study has examined the effect of matrix cracks and delamination on extension-twist coupling of thin pretwisted composite strips. The modeling strategy adopted in the study combines the capability of computational micromechanics and continuum damage mechanics to characterize cracked plies and sublaminates approach to account for delamination within the structural modeling framework based on VAM. After validating the model for determining the degraded modulus - both longitudinal and transverse, shear modulus and Poisson's ratio for different layups and matrix crack densities and axial-twist response for a delaminated strip with Winckler layup against experimental results, the effect of damage on trapeze effect was studied. Detailed investigations were undertaken for three different cases: (i) strips with only matrix cracks; (ii) strips with only mid-surface edge delamination; and (iii) strips with matrix cracks and mid-surface edge delamination. In all the cases pretwisted strips with Winckler layup was considered. The results can be summarized as follows:

- A nonlinear relationship between the end-twist and the applied axial force was observed in all the three cases studied. However, it was observed that type of defect can affect the nature of the extension-twist coupling behavior of the strip. For the case of strips having only matrix cracks, the coupling increased with increase in crack density. In strips with only delamination, the coupling reduced with increase in the size of mid-surface edge delamination. Strips having both matrix cracks and delamination showed reduced extension-twist coupling.
- In strips having only matrix cracks, the presence of matrix cracks leads to the degradation of individual ply properties. However, the cross-sectional stiffness terms directly influencing the extension-twist coupling are not significantly affected. Hence, increase in the end twist for a given axial load can be primarily attributed to stiffness degradation at the individual ply level.
- In strips having only delamination, it was observed that the presence of delamination reduces the cross-sectional stiffness terms influencing the extension-twist coupling. As delamination size increases, the behavior of the strip is dominated by the two symmetric sublaminates, above and below the delamination, leading to significant reduction in the extension-twist coupling. The coupling vanishes if the strip is completely delaminated.
- Finally, in strips having matrix cracks and delamination, the coupling behavior is sensitive to the delamination size more than the crack density. Delamination size determines the extent of overall extension-twist stiffness reduction and consequently affects the coupling behavior.

## Appendix A

The healthy linear stiffness terms are,

$$S_{11} = b\bar{\bar{A}}_{11}^h$$

$$S_{12} = \frac{1}{12}b^3k_1\bar{\bar{A}}_{11}^h - 2b\bar{\bar{B}}_{16}^h$$

$$S_{13} = b\bar{\bar{B}}_{11}^h$$

$$S_{14} = 0$$

$$S_{22} = \frac{1}{80}b^5k_1^2\bar{\bar{A}}_{11}^h - \frac{1}{3}b^3k_1\bar{\bar{B}}_{16}^h + 4b\bar{\bar{D}}_{66}^h$$

$$S_{23} = \frac{1}{12}b^3k_1\bar{\bar{B}}_{11}^h - 2b\bar{\bar{D}}_{16}^h$$

$$S_{24} = 0$$

$$S_{33} = b\bar{\bar{D}}_{11}^h$$

$$S_{34} = 0$$

$$S_{44} = \frac{1}{12}b^3\bar{\bar{A}}_{11}^h$$

The healthy nonlinear stiffness terms are,

$$S_{15} = \frac{1}{24}b^3\bar{\bar{A}}_{11}^h$$

$$S_{16} = S_{17} = S_{18} = S_{19} = 0$$

$$S_{25} = \frac{1}{480}(3b^5k_1\bar{\bar{A}}_{11}^h - 40b^3\bar{\bar{B}}_{16}^h)$$

$$S_{26} = \frac{b^5k_1\bar{\bar{A}}_{11}^h\bar{\bar{D}}_{12}^h}{360\bar{\bar{D}}_{22}^h}$$

$$S_{27} = \frac{b^5k_1\bar{\bar{A}}_{11}^h\bar{\bar{B}}_{12}^h}{360\bar{\bar{D}}_{22}^h}$$

$$S_{28} = S_{29} = 0$$

$$S_{35} = \frac{b^5k_1\bar{\bar{A}}_{11}^h(b^2k_1\bar{\bar{B}}_{12}^h - 56\bar{\bar{B}}_{26}^h) + 420b^3\bar{\bar{B}}_{11}^h\bar{\bar{D}}_{22}^h}{10080\bar{\bar{D}}_{22}^h}$$

$$S_{36} = S_{37} = S_{38} = S_{39} = S_{45} = S_{46} = S_{47} = 0$$

$$S_{48} = -\frac{b^5\bar{\bar{A}}_{11}^h\bar{\bar{B}}_{12}^h}{720\bar{\bar{D}}_{22}^h}$$

$$S_{49} = 0$$

$$S_{55} = \frac{1}{320}b^5\bar{\bar{A}}_{11}^h$$

$$S_{56} = 0$$

$$S_{57} = \frac{b^5\bar{\bar{A}}_{11}^h\bar{\bar{B}}_{12}^h}{720\bar{\bar{D}}_{22}^h}$$

$$S_{58} = 0$$

$$S_{59} = \frac{b^5\bar{\bar{A}}_{11}^h(b^2k_1\bar{\bar{B}}_{12}^h - 28\bar{\bar{B}}_{26}^h)}{10080\bar{\bar{D}}_{22}^h}$$

$$S_{66} = \frac{b^5\bar{\bar{A}}_{11}^h\bar{\bar{D}}_{12}^h{}^2}{720\bar{\bar{D}}_{22}^h{}^2}$$

$$S_{67} = \frac{b^5\bar{\bar{A}}_{11}^h\bar{\bar{B}}_{12}^h\bar{\bar{D}}_{12}^h}{720\bar{\bar{D}}_{22}^h{}^2}$$

$$S_{68} = 0$$

$$S_{69} = -\frac{b^5\bar{\bar{A}}_{11}^h\bar{\bar{D}}_{12}^h(b^2k_1\bar{\bar{B}}_{12}^h + 168\bar{\bar{B}}_{26}^h)}{60480\bar{\bar{D}}_{22}^h{}^2}$$

$$S_{77} = \frac{b^5\bar{\bar{A}}_{11}^h\bar{\bar{B}}_{12}^h{}^2}{720\bar{\bar{D}}_{22}^h{}^2}$$

$$S_{78} = 0$$

$$S_{79} = -\frac{b^5\bar{\bar{A}}_{11}^h\bar{\bar{B}}_{12}^h(b^2k_1\bar{\bar{B}}_{12}^h + 168\bar{\bar{B}}_{26}^h)}{60480\bar{\bar{D}}_{22}^h{}^2}$$

$$S_{88} = -\frac{b^7\bar{\bar{A}}_{11}^h(\bar{\bar{A}}_{11}^h\bar{\bar{D}}_{22}^h - 3\bar{\bar{B}}_{12}^h{}^2)}{30240\bar{\bar{D}}_{22}^h{}^2}$$

$$S_{89} = 0$$

$$S_{99} = \frac{1}{3628800\bar{\bar{D}}_{22}^h{}^2} \left[ b^5\bar{\bar{A}}_{11}^h \left\{ -b^4k_1^2(40\bar{\bar{A}}_{11}^h\bar{\bar{D}}_{22}^h + 9\bar{\bar{B}}_{12}^h{}^2)\bar{\bar{B}}_{26}^h + 240b^2k_1\bar{\bar{B}}_{12}^h + 10080(2\bar{\bar{B}}_{26}^h{}^2 + \bar{\bar{D}}_{12}^h\bar{\bar{D}}_{22}^h) \right\} \right]$$

The new stiffness variables used above (the quantities with a double overbar and overbar) are defined in the [Appendix C](#).

## Appendix B

The terms in the delaminated linear stiffness matrix are,

$$\begin{aligned} S_{11} &= 2a\bar{\bar{A}}_{11}^h + \bar{A}_{11}^d(2b - 4a) \\ S_{12} &= \frac{1}{6} \left\{ 4a(a^2 k_1 \bar{\bar{A}}_{11}^h - 6\bar{\bar{B}}_{16}^h) + \bar{A}_{11}^d k_1 (b^3 - 8a^3) \right\} \\ S_{13} &= S_{14} = 0 \\ S_{22} &= \frac{1}{120\bar{D}_{22}^d} \left[ \bar{D}_{22}^d \left\{ 16a(3a^4 k_1^2 \bar{\bar{A}}_{11}^h - 20a^2 k_1 \bar{\bar{B}}_{16}^h + 60\bar{\bar{D}}_{66}^h) \right. \right. \\ &\quad \left. \left. + 3\bar{A}_{11}^d k_1^2 (b^5 - 32a^5) - 960\bar{D}_{66}^d (2a - b) \right\} + 960\bar{D}_{26}^d{}^2 (2a - b) \right] \\ S_{23} &= S_{24} = 0 \\ S_{33} &= 2a\bar{\bar{D}}_{11}^h + \bar{D}_{11}^d(2b - 4a) + \frac{4a\bar{D}_{12}^d{}^2}{\bar{D}_{22}^d} - \frac{2b\bar{D}_{12}^d{}^2}{\bar{D}_{22}^d} \\ S_{34} &= 0 \\ S_{44} &= \frac{1}{6} \left\{ 4a^3 \bar{\bar{A}}_{11}^h + \bar{A}_{11}^d (b^3 - 8a^3) \right\} \end{aligned}$$

The terms in the delaminated nonlinear stiffness matrix are,

$$\begin{aligned} S_{15} &= \frac{1}{12} \left\{ 4a^3 \bar{\bar{A}}_{11}^h + \bar{A}_{11}^d (b^3 - 8a^3) \right\} \\ S_{16} &= -\frac{a(2a - b)(\bar{A}_{11}^d - \bar{\bar{A}}_{11}^h) \left\{ 2a\bar{D}_{22}^d \bar{D}_{12}^h (2a - 3b) - \bar{D}_{12}^d \bar{D}_{22}^h (b - 2a)^2 \right\}}{12\bar{D}_{22}^d \bar{D}_{22}^h (a - b)} \\ S_{17} &= S_{18} = S_{19} = 0 \\ S_{25} &= \frac{1}{5} a^5 k_1 \bar{\bar{A}}_{11}^h - \frac{2}{3} a^3 \bar{\bar{B}}_{16}^h - \frac{1}{80} \bar{A}_{11}^d k_1 (32a^5 - b^5) \\ S_{26} &= -\frac{1}{720\bar{D}_{22}^d \bar{D}_{22}^h (a - b)} \\ &\quad \times \left[ 4a \left\{ 2a\bar{D}_{22}^d \bar{D}_{12}^h \left( a^2 k_1 \bar{\bar{A}}_{11}^h (-28a^2 + 48ab - 15b^2) \right. \right. \right. \\ &\quad \left. \left. + 30\bar{\bar{B}}_{16}^h (4a^2 - 8ab + 3b^2) \right\} \right. \\ &\quad \left. + 5\bar{D}_{12}^d \bar{D}_{22}^h (2a - b)^3 \left( a^2 k_1 \bar{\bar{A}}_{11}^h - 6\bar{\bar{B}}_{16}^h \right) \right\} \\ &\quad + \text{Ad}_{11} k_1 (2a - b) \left\{ 5a\bar{D}_{22}^d \bar{D}_{12}^h (40a^4 - 52a^3 b - 2a^2 b^2 + 3ab^3 - 3b^4) \right. \\ &\quad \left. - \bar{D}_{12}^d \bar{D}_{22}^h (b - 2a)^2 (34a^3 - 3a^2 b + 4b^3) \right\} \right] \\ S_{27} &= S_{28} = S_{29} = S_{35} = S_{36} = 0 \\ S_{37} &= -\frac{a(2a - b)(\bar{A}_{11}^d - \bar{\bar{A}}_{11}^h) \left\{ 2a\bar{D}_{22}^d \bar{D}_{12}^h (2a - 3b) - \bar{D}_{12}^d \bar{D}_{22}^h (b - 2a)^2 \right\}}{12\bar{D}_{22}^d \bar{D}_{22}^h (a - b)} \\ S_{38} &= S_{39} = S_{45} = S_{46} = S_{47} = S_{48} = S_{49} = 0 \\ S_{55} &= \frac{1}{160} \left\{ 16a^5 \bar{\bar{A}}_{11}^h + \bar{A}_{11}^d (b^5 - 32a^5) \right\} \\ S_{56} &= S_{57} = S_{58} = S_{59} = 0 \\ S_{66} &= \frac{1}{1440\bar{D}_{22}^d{}^2 \bar{D}_{22}^h{}^2 (a - b)^2} \\ &\quad \times \left[ a\bar{\bar{A}}_{11}^h \left\{ 4a^2 \bar{D}_{22}^d{}^2 \bar{D}_{12}^h{}^2 (96a^4 - 352a^3 b + 456a^2 b^2 \right. \right. \\ &\quad \left. \left. - 240ab^3 + 45b^4) + 5\bar{D}_{12}^d{}^2 \bar{D}_{22}^h{}^2 (b - 2a)^6 \right. \right. \\ &\quad \left. \left. - 20a\bar{D}_{12}^d \bar{D}_{22}^d \bar{D}_{12}^h \bar{D}_{22}^h (2a - 3b) (b - 2a)^4 \right\} \right. \\ &\quad \left. - \bar{A}_{11}^d (2a - b) \left\{ \bar{D}_{12}^d{}^2 \bar{D}_{22}^h{}^2 (9a^2 - 8ab + 4b^2) (b - 2a)^4 \right. \right. \\ &\quad \left. \left. - 10a\bar{D}_{12}^d \bar{D}_{22}^d \bar{D}_{12}^h \bar{D}_{22}^h (10a^3 - 21a^2 b + 12ab^2 - 3b^3) (b - 2a)^2 \right. \right. \\ &\quad \left. \left. + 20a^2 (\bar{D}_{22}^d)^2 \bar{D}_{12}^h{}^2 (16a^4 - 48a^3 b + 48a^2 b^2 - 18ab^3 + 3b^4) \right\} \right] \\ S_{67} &= S_{68} = S_{69} = S_{77} = S_{78} = S_{89} = 0 \end{aligned}$$

$$\begin{aligned} S_{79} &= -\frac{1}{80640\bar{D}_{22}^d \bar{D}_{22}^h (a - b)} \left[ ak_1 (2a - b) (\bar{A}_{11}^d - \bar{\bar{A}}_{11}^h) \right. \\ &\quad \times \left\{ 256a^5 \bar{D}_{22}^d \bar{\bar{A}}_{11}^h (7b - 2a) + \bar{A}_{11}^d (2a - b)^3 \right. \\ &\quad \left. \left. \times \left( 70a\bar{D}_{22}^d (4a^2 - 4ab - 3b^2) - \bar{D}_{22}^h (b - 2a)^2 (54a + 29b) \right) \right\} \right] \\ S_{88} &= \frac{1}{967680b^2 \bar{D}_{22}^d \bar{D}_{22}^h (a - b)} \\ &\quad \times \left[ 2048a^7 (\bar{\bar{A}}_{11}^h)^2 \left\{ \bar{D}_{22}^d (140a^3 - 135ab^2 + 51b^3) - 35\bar{D}_{22}^h (2a - b)^3 \right\} \right. \\ &\quad \left. - 112a^3 \bar{A}_{11}^d \bar{\bar{A}}_{11}^h (b - 2a)^2 \left\{ 16a^2 \bar{D}_{22}^d (20a^3 + 180a^2 b - 35ab^2 - 48b^3) \right. \right. \\ &\quad \left. \left. - \bar{D}_{22}^h (b - 2a)^2 (160a^3 + 580a^2 b + 392ab^2 + 29b^3) \right\} \right. \\ &\quad \left. + \bar{A}_{11}^d{}^2 (2a - b)^5 \left\{ 280a^3 \bar{D}_{22}^d (2a^2 + 37ab + 17b^2) \right. \right. \\ &\quad \left. \left. - \bar{D}_{22}^h (1120a^5 + 8120a^4 b + 1396a^3 b^2 - 2330a^2 b^3 - 271ab^4 + b^5) \right\} \right] \\ S_{99} &= -\frac{1}{5806080\bar{D}_{22}^d{}^2 \bar{D}_{22}^h (a - b)} \\ &\quad \times \left[ 512a^3 \bar{D}_{22}^d \bar{\bar{A}}_{11}^h \left\{ 2a\bar{D}_{22}^d (-72a^2 k_1 \bar{\bar{B}}_{16}^h (4a^2 - 16ab + 7b^2) \right. \right. \\ &\quad \left. \left. - 63\bar{D}_{12}^h (28a^2 - 48ab + 15b^2) + 4a^4 k_1^2 \bar{\bar{A}}_{11}^h (20a^2 - 56ab + 21b^2) \right\} \right. \\ &\quad \left. + 315\bar{D}_{12}^d \bar{D}_{22}^h (2a - b)^3 \right\} \\ &\quad - 48\bar{A}_{11}^d (2a - b) \left\{ -\bar{D}_{22}^d \bar{D}_{22}^h (b - 2a)^2 \right. \\ &\quad \left. \times \left( ak_1 (2a - b)^3 (54a + 29b) (a^2 k_1 \bar{\bar{A}}_{11}^h - 6\bar{\bar{B}}_{16}^h) \right. \right. \\ &\quad \left. \left. - 168\bar{D}_{12}^d (34a^3 - 3a^2 b + 4b^3) \right) \right. \\ &\quad \left. + 2a\bar{D}_{22}^d{}^2 (-210ak_1 \bar{\bar{B}}_{16}^h (2a - b)^3 (4a^2 - 4ab - 3b^2) \right. \\ &\quad \left. - 420\bar{D}_{12}^h (40a^4 - 52a^3 b - 2a^2 b^2 + 3ab^3 - 3b^4) \right. \\ &\quad \left. + a^3 k_1^2 \bar{\bar{A}}_{11}^h (2272a^5 - 4912a^4 b + 1520a^3 b^2 + 392a^2 b^3 - 602ab^4 \right. \\ &\quad \left. + 105b^5) - 3024\bar{D}_{26}^d{}^2 \bar{D}_{22}^h (a - b) (b - 2a)^4 \right\} \\ &\quad \left. + (\bar{A}_{11}^d)^2 \bar{D}_{22}^d k_1^2 (b - 2a)^4 \right. \\ &\quad \left. \times \left\{ 105a\bar{D}_{22}^d (272a^5 - 208a^4 b - 200a^3 b^2 - 8a^2 b^3 - 15ab^4 - 9b^5) \right. \right. \\ &\quad \left. \left. - 2\bar{D}_{22}^h (b - 2a)^2 (1724a^4 + 1168a^3 b + 315a^2 b^2 + 215ab^3 + 64b^4) \right\} \right] \end{aligned}$$

The new stiffness variables used above (the quantities with a double overbar and overbar) are defined in the [Appendix C](#).

## Appendix C

The new healthy stiffness variables (the quantities with a over doublebar)

$$\begin{aligned} \bar{\bar{A}}_{11}^h &= \bar{A}_{11}^h - \frac{\bar{B}_{12}^h{}^2}{\bar{D}_{22}^h} \\ \bar{\bar{B}}_{11}^h &= \bar{B}_{11}^h - \frac{\bar{B}_{12}^h \bar{D}_{12}^h}{\bar{D}_{22}^h} \\ \bar{\bar{B}}_{16}^h &= \bar{B}_{16}^h - \frac{\bar{B}_{12}^h \bar{D}_{26}^h}{\bar{D}_{22}^h} \\ \bar{\bar{D}}_{11}^h &= \bar{D}_{11}^h - \frac{\bar{D}_{12}^h{}^2}{\bar{D}_{22}^h} \\ \bar{\bar{D}}_{16}^h &= \bar{D}_{16}^h - \frac{\bar{D}_{12}^h \bar{D}_{26}^h}{\bar{D}_{22}^h} \\ \bar{\bar{D}}_{66}^h &= \bar{D}_{66}^h - \frac{\bar{D}_{26}^h{}^2}{\bar{D}_{22}^h} \end{aligned}$$

The new healthy stiffness variables (the quantities with an overbar)

$$\begin{aligned}\bar{A}_{11}^h &= A_{11}^h + \frac{A_{16}^h{}^2 A_{22}^h - 2A_{12}^h A_{16}^h A_{26}^h + A_{12}^h{}^2 A_{66}^h}{A_{26}^h{}^2 - A_{22}^h A_{66}^h} \\ \bar{B}_{11}^h &= B_{11}^h + \frac{A_{12}^h A_{66}^h B_{12}^h + A_{16}^h A_{22}^h B_{16}^h - A_{16}^h (A_{16}^h B_{12}^h + A_{12}^h B_{16}^h)}{A_{26}^h{}^2 - A_{22}^h A_{66}^h} \\ \bar{B}_{12}^h &= B_{12}^h + \frac{A_{12}^h A_{66}^h B_{22}^h + A_{16}^h A_{22}^h B_{26}^h - A_{26}^h (A_{16}^h B_{22}^h + A_{12}^h B_{26}^h)}{A_{26}^h{}^2 - A_{22}^h A_{66}^h} \\ \bar{B}_{16}^h &= B_{16}^h + \frac{A_{12}^h A_{66}^h B_{26}^h + A_{16}^h A_{22}^h B_{66}^h - A_{26}^h (A_{16}^h B_{26}^h + A_{12}^h B_{66}^h)}{A_{26}^h{}^2 - A_{22}^h A_{66}^h} \\ \bar{D}_{11}^h &= D_{11}^h + \frac{A_{66}^h B_{12}^h{}^2 - 2A_{26}^h B_{12}^h B_{16}^h + A_{22}^h B_{16}^h{}^2}{A_{26}^h{}^2 - A_{22}^h A_{66}^h} \\ \bar{D}_{12}^h &= D_{12}^h + \frac{A_{66}^h B_{12}^h B_{22}^h + A_{22}^h B_{16}^h B_{26}^h - A_{26}^h (B_{16}^h B_{22}^h + B_{12}^h B_{26}^h)}{A_{26}^h{}^2 - A_{22}^h A_{66}^h} \\ \bar{D}_{22}^h &= D_{22}^h + \frac{A_{66}^h B_{22}^h{}^2 - 2A_{26}^h B_{22}^h B_{26}^h + A_{22}^h B_{26}^h{}^2}{A_{26}^h{}^2 - A_{22}^h A_{66}^h} \\ \bar{D}_{16}^h &= D_{16}^h + \frac{A_{66}^h B_{12}^h B_{26}^h + A_{22}^h B_{16}^h B_{66}^h - A_{26}^h (B_{16}^h B_{26}^h + B_{12}^h B_{66}^h)}{A_{26}^h{}^2 - A_{22}^h A_{66}^h} \\ \bar{D}_{26}^h &= D_{26}^h + \frac{A_{66}^h B_{22}^h B_{26}^h + A_{22}^h B_{26}^h B_{66}^h - A_{26}^h (B_{26}^h{}^2 + B_{22}^h B_{66}^h)}{A_{26}^h{}^2 - A_{22}^h A_{66}^h} \\ \bar{D}_{66}^h &= D_{66}^h + \frac{A_{66}^h B_{26}^h{}^2 - 2A_{26}^h B_{26}^h B_{66}^h + A_{22}^h B_{66}^h{}^2}{A_{26}^h{}^2 - A_{22}^h A_{66}^h}\end{aligned}$$

By replacing the superscript 'h' by 'd' and taking note of the fact that the delaminated sublaminates is symmetric, we get the modified stiffness definitions for the delaminated sublaminates.

## References

- [1] Friedmann PP. Rotary-wing aeroelasticity: current status and future trends. *AIAA J* 2004;42(10):1953–72.
- [2] Bousman WG, Ormiston RA, Mirick PH. Design considerations for bearingless rotor hubs. Technical report, DTIC Document; 1983.
- [3] Flagg DL, Kural MH. Experimental determination of the in situ transverse lamina strength in graphite/epoxy laminates. *J Compos Mater* 1982;16(2):103–16.
- [4] Talreja R. Continuum mechanics characterization of damage in composite materials. *Proc R Soc London, Series A: Math Phys Sci* 1985;399:195–216.
- [5] Hashin Z. Analysis of cracked laminates: a variational approach. *Mech Mater* 1985;4(2):121–36.
- [6] Ladevèze P, LeDantec E. Damage modelling of the elementary ply for laminated composites. *Compos Sci Technol* 1992;43(3):257–67.
- [7] Kashtalyan M, Soutis C. Stiffness degradation in cross-ply laminates damaged by transverse cracking and splitting. *Composites Part A* 2000;31(4):335–51.
- [8] Camanho PP, Mayugo JA, Maimí P. A micromechanics-based damage model for composite laminates. *Multiscale Behav Mater Struct: Anal, Numer Exp Simul* 2006;6:1.
- [9] Montesano J, Singh CV. A synergistic damage mechanics based multiscale model for composite laminates subjected to multiaxial strains. *Mech Mater* 2015;83:72–89.
- [10] Talreja R. Physical modelling of failure in composites. *Philos Trans R Soc A: Math, Phys Eng Sci* 2016;374(2071).
- [11] Highsmith AL, Reifsnider KL. Stiffness-reduction mechanisms in composite laminates. *Damage Compos Mater, ASTM STP* 1982;775:103–17.
- [12] Nairn JA. The strain energy release rate of composite microcracking: a variational approach. *J Compos Mater* 1989;23(11):1106–29.
- [13] Hajikazemi M, Sadr MH. Stiffness reduction of cracked general symmetric laminates using a variational approach. *Int J Solids Struct* 2014;51(7–8):1483–93.
- [14] Gudmundson P, Ostlund S. First order analysis of stiffness reduction due to matrix cracking. *J Compos Mater* 1992;26(7):1009–30.
- [15] Varna J, Joffe R, Akshantala NV, Talreja R. Damage in composite laminates with off-axis plies. *Compos Sci Technol* 1999;59(14):2139–47.
- [16] Lundmark P, Varna J. Constitutive relationships for laminates with ply cracks in in-plane loading. *Int J Damage Mech* 2005;14(3):235–59.
- [17] Lundmark P, Varna J. Crack face sliding effect on stiffness of laminates with ply cracks. *Compos Sci Technol* 2006;66(10):1444–54.
- [18] Talreja R. Stiffness properties of composite laminates with matrix cracking and interior delamination. *Eng Fract Mech* 1986;25(5–6):751–62.
- [19] Allen DH, Harris CE, Groves SE. A thermomechanical constitutive theory for elastic composites with distributed damage-i. Theoretical development. *Int J Solids Struct* 1987;23(9):1301–18.
- [20] Maimí P, Camanho PP, Mayugo JA, Dávila CG. A continuum damage model for composite laminates: part i – constitutive model. *Mech Mater* 2007;39(10):897–908.
- [21] Maimí P, Camanho PP, Mayugo JA, Dávila CG. A continuum damage model for composite laminates: part ii – computational implementation and validation. *Mech Mater* 2007;39(10):909–19.
- [22] Garrett KW, Bailey JE. Multiple transverse fracture in 90° cross-ply laminates of a glass fibre-reinforced polyester. *J Mater Sci* 1977;12(1):157–68.
- [23] Laws N, Dvorak GJ. Progressive transverse cracking in composite laminates. *J Compos Mater* 1988;22(10):900–16.
- [24] Asadi A, Raghavan J. Model for evolution of quasi-static transverse cracking in multiple plies of multidirectional polymer composite laminates. *Compos Struct* 2015;132:665–79.
- [25] Berthelot J. Transverse cracking and delamination in cross-ply glass-fiber and carbon-fiber reinforced plastic laminates: static and fatigue loading. *Appl Mech Rev* 2003;56(1):111–47.
- [26] Li S, Reid SR, Soden PD. A continuum damage model for transverse matrix cracking in laminated fibre-reinforced composites. *Philos Trans R Soc A: Math, Phys Eng Sci* 1998;356(1746):2379–412.
- [27] Barbero EJ, Abdelal GF, Caceres A. A micromechanics approach for damage modeling of polymer matrix composites. *Compos Struct* 2005;67(4):427–36.
- [28] Maimí P, Camanho PP, Mayugo JA, Dávila CG. A continuum damage model for composite laminates: part i – constitutive model. *Mech Mater* 2007;39(10):897–908.
- [29] Montesano J, Chu H, Singh CV. Development of a physics-based multi-scale progressive damage model for assessing the durability of wind turbine blades. *Compos Struct* 2016;141:50–62.
- [30] Singh CV, Talreja R. A synergistic damage mechanics approach for composite laminates with matrix cracks in multiple orientations. *Mech Mater* 2009;41(8):954–68.
- [31] Della CN, Shu D. Vibration of delaminated composite laminates: a review. *Appl Mech Rev* 2007;60(1–6):1–20.
- [32] Mujumdar PM, Suryanarayan S. Flexural vibrations of beams with delaminations. *J Sound Vib* 1988;125(3):441–61.
- [33] Kim KS, Hong CS. Delamination growth in angle-ply laminated composites. *J Compos Mater* 1986;20(5):423–38.
- [34] Wang W, Song H, Xue J, Guo W, Zheng M. Overview of intelligent composites with embedded fbg sensors. In: Proceedings of the 2011 IEEE 5th international conference on cybernetics and intelligent systems, CIS 2011; 2011. p. 47–51.
- [35] Barbero EJ, Reddy JN. Modeling of delamination in composite laminates using a layer-wise plate theory. *Int J Solids Struct* 1991;28(3):373–88.
- [36] Saravanan DA, Hopkins DA. Effects of delaminations on the damped dynamic characteristics of composite laminates: analysis and experiments. *J Sound Vib* 1996;192(5):977–93.
- [37] Shen MH, Grady JE. Free vibrations of delaminated beams. *AIAA J* 1992;30(5):1361–70.
- [38] Armanios EA, Rehfield LW. Interlaminar analysis of laminated composites using a sublaminates approach. In: Collection of technical papers – AIAA/ASME/ASCE/AHS/ASC structures, structural dynamics and materials conference, vol. 1; 1986. p. 442–52.
- [39] Li S, Reid SR, Soden PD. A finite strip analysis of cracked laminates. *Mech Mater* 1994;18(4):289–311.
- [40] Chakraborty A, Roy Mahapatra D, Gopalakrishnan S. Finite element analysis of free vibration and wave propagation in asymmetric composite beams with structural discontinuities. *Compos Struct* 2002;55(1):23–36.
- [41] Averill RC. Static and dynamic response of moderately thick laminated beams with damage. *Compos Eng* 1994;4(4):381–95.
- [42] Kim HS, Chattopadhyay A, Ghoshal A. Characterization of delamination effect on composite laminates using a new generalized layerwise approach. *Comput Struct* 2003;81(15):1555–66.
- [43] Cho M. Higher-order zig-zag theory for laminated composites with multiple delaminations. *J Appl Mech, Trans ASME* 2001;68(6):869–77.
- [44] Carrera E. Theories and finite elements for multilayered, anisotropic, composite plates and shells. *Arch Comput Methods Eng* 2002;9(2):87–140.
- [45] Carrera E. Theories and finite elements for multilayered plates and shells: a unified compact formulation with numerical assessment and benchmarking. *Arch Comput Methods Eng* 2003;10(3).
- [46] Keshava Kumar S, Cinefra M, Carrera E, Ganguli R, Harursampath D. Finite element analysis of free vibration of the delaminated composite plate with variable kinematic multilayered plate elements. *Compos Part B: Eng* 2014;66:453–65.
- [47] Cesnik CES, Hodges DH. Stiffness constants for composite beams including large initial twist and curvature effects. *Appl Mech Rev* 1995;48(11/2):S61–7.
- [48] Yu W, Hodges DH, Volovoi V, Cesnik CES. On timoshenko-like modeling of initially curved and twisted composite beams. *Int J Solids Struct* 2002;39(19):5101–21.
- [49] Hodges DH. Geometrically exact, intrinsic theory for dynamics of curved and twisted anisotropic beams. *AIAA J* 2003;41(6):1131–7.
- [50] Berdichevskii VL. Variational-asymptotic method of constructing a theory of shells. *PMM, vol. 43, no. 4, 1979, pp. 664–687. J Appl Math Mech* 1979;43(4):711–36.

- [51] Hodges DH. A mixed variational formulation based on exact intrinsic equations for dynamics of moving beams. *Int J Solids Struct* 1990;26(11):1253–73.
- [52] Hodges DH, Lee BW, Atilgan AR. Application of the variational-asymptotical method to laminated composite plates. *AIAA J* 1993;31(9):1674–83.
- [53] Hodges DH, Harursampath D, Volovoi VV, Cesnik CES. Non-classical effects in non-linear analysis of pretwisted anisotropic strips. *Int J Non Linear Mech* 1999;34(2):259–77.
- [54] Harursampath D, Hodges DH. Asymptotic analysis of the non-linear behavior of long anisotropic tubes. *Int J Non Linear Mech* 1999;34(6):1003–18.
- [55] Yu W, Hodges DH. A geometrically nonlinear shear deformation theory for composite shells. *J Appl Mech, Trans ASME* 2004;71(1):1–9.
- [56] Jiang F, Yu W. Nonlinear variational asymptotic sectional analysis of hyperelastic beams. *AIAA J* 2016;54(2):679–90.
- [57] Guruprasad PJ, Thejasvi M, Harursampath D. Nonlinear analysis of a thin pretwisted and delaminated anisotropic strip. *Acta Mech* 2014;225(10):2815–32.
- [58] Pollayi H, Yu W. Modeling matrix cracking in composite rotor blades within vabs framework. *Compos Struct* 2014;110(1):62–76.
- [59] Makeev A, Armanios EA. A geometrically nonlinear model for laminated composite strips with extension-twist coupling in the presence of delamination. *J Appl Mech, Trans ASME* 1998;65(3):685–93.
- [60] Armanios EA, Makeev A, Hooke D. Finite-displacement analysis of laminated composite strips with extension-twist coupling. *J Aerosp Eng* 1996;9(3):80–91.
- [61] Danielson DA, Hodges DH. Nonlinear beam kinematics by decomposition of the rotation tensor. *J Appl Mech, Trans ASME* 1987;54(2):258–62.
- [62] Singh CV, Talreja R. Evolution of ply cracks in multidirectional composite laminates. *Int J Solids Struct* 2010;47(10):1338–49.
- [63] Tong J, Guild FJ, Ogin SL, Smith PA. On matrix crack growth in quasi-isotropic laminates – I. Experimental investigation. *Compos Sci Technol* 1997;57(11):1527–35.
- [64] Lee JH, Hong CS. Refined two-dimensional analysis of cross-ply laminates with transverse cracks based on the assumed crack opening deformation. *Compos Sci Technol* 1993;46(2):157–66.
- [65] Groves SE, Harris CE, Highsmith AL, Allen DH, Norvell RG. An experimental and analytical treatment of matrix cracking in cross-ply laminates. *Exp Mech* 1987;27(1):73–9.